An Experimental Study of Scour Process and Sediment Transport around a Bridge Pier with Foundation

S. Umeda[1], T. Yamazaki[2] and M. Yuhi[3]

[1]School of Environmental Design, Kanazawa University, Kakuma-machi, Kanazawa, 920-1192, Japan; Tel.:+81-76-234-4606; e-mail:umeda@t.kanazawa-u.ac.jp
[2]Kanto branch office, East Japan Expressway Ltd., 2-101-1, Banshoumen, Misato, 341-0056, Japan; Tel.:+81-48-952-8561; e-mail: t.yamazaki.ae@e-nexco.co.jp
[3]School of Environmental Design, Kanazawa University, Kakuma-machi, Kanazawa, 920-1192, Japan; Tel.:+81-76-234-4609; e-mail: yuhi@t.kanazawa-u.ac.jp

ABSTRACT

Laboratory experiments were conducted on the time development of clear water scour around a non-uniform cylindrical pier in steady flow. The pier comprised a slender cylinder founded on a large cylinder. This study aimed at investigating the effects of foundation depth on the scour process. Three-dimensional topography of the scour was carefully measured using digital stereo-photogrammetry as a method to level a riverbed. The spatial distributions of the sediment transport rate were estimated with the variation in the bed elevation. The results show that the process of sediment transport and scour depends on the foundation depth. The retarding and limiting the scour due to the foundation occur when it is placed at an appropriate level below the initial bed level. The scour depth increases with foundation level when the foundation protrudes above the initial bed level.

INTRODUCTION

Scour around the foundations of bridge piers is one of the major causes of serious damage to bridges (e.g. Tsujimoto et al., 1987). Since most rivers in Japan have been under severe bed degradation, it can be considered that there are many bridge piers at risk of exposure of its foundation during floods. Considerable understanding of flow and scour around a cylindrical pier has been achieved by a great many experimental research works over a long time. Previous scour investigators mainly focused on the scour around piers of uniform horizontal cross-section geometry and did not consider the effects of foundation geometry. In practice, foundations often exposed to flow and constitute a significant part of the obstruction that causes local scour.

Several investigations are available those describe the scour around piers of nonuniform geometry in consideration of the foundation. However, most of them focus on the formulation of maximum scour depth equations (e.g. Melville & Raudkivi, 1996) or the analytical modeling of the scour depth (e.g. Tsujimoto et al., 1987; Lu et al., 2008). Few investigators have described the mechanism of scour at a pier with foundation. Little is known about the effect of foundation depth on scour process. Further experimental investigations concerning the sediment transport around a nonuniform pier are needed for a deeper understanding of the mechanism of local scour. The purpose of this study is to examine the influence of foundation depth on the process of the scour development and sediment transport around a pier with foundation.

EXPERIMENTAL SETUP

Experiments were conducted in a flume 12 m in length, 0.4 m wide and 0.4 m deep. Scouring tests were carried out in a sediment recess section situated 7.5 m from the inlet. The recess was 2.5 m in length, 0.4 m wide and 0.14 m deep. Refer to Umeda et al. (2008) for detailed description on the flume setup. A uniformly graded fine sand of mean diameter d_{50} = 0.17 mm was used to simulate the process of scour and sediment transport for a bed of cohesionless sediment. A model of a bridge pier with foundation shown in Figure 1 was mounted on the flume bed on the centerline. The pier was simply modeled with a slender cylinder (D = 30 mm) founded on a large cylinder (D^* = 50 mm). The foundation top elevation Z shown in Figure 1 is measured from the initial bed level and is positive if the top of the foundation is below the initial bed level and vice versa. Scouring tests were performed under a clear water scouring condition. The mean water depth h = 0.147 m, the mean flow velocity U_m = 0.17 m/s, the mean water temperature was 25 °C. The Froude number was F_r = 0.14. The pier Reynolds number was Re_D = 5700. While the Shields parameter estimated from the velocity profile of undisturbed flow was θ_0 = 0.04, the critical Shields parameter for the mobilization of the sediment war θ_c = 0.05. The tests were run for 4 or 5 days until the variation in the scour depth was less than 5% of the pier diameter in the succeeding 24 hours.

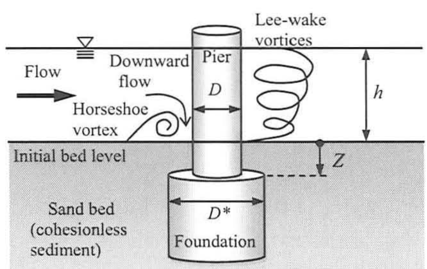

Figure 1. Model of bridge pier and relative foundation depth, *Z/D*.

MEASURING TECHNIQUE

Three-dimensional topography of the scoured bed (cf. Figure 4) was measured by digital stereo-photogrammetry. This technique is essentially based upon the concept of triangulation, in which three-dimensional object points can be determined from corresponding image points from at least two perspectives. This technique can determine scoured bed elevations around the pier with foundation. Four perspectives were taken from different directions to provide four stereo-pairs of images for accurately estimating the bed geometry near the pier (cf. Umeda et al., 2008). The images were taken, after shutting off and trapping water in the flume.

To validate the accuracy of the stereo-photogrammetric system on an underwater condition, initial tests were carried out by using the calibration target

Table 1. Accuracy of the stereo-photogrammetric system on the underwater condition for 0.15m in depth.

	Estimation (A) mm	Measurement (B) mm	Absolute error (C=|A−B|) mm	Rate of error (D=100C/A) %
Horizontal dimensions Xa	53.7	54.0	0.3	0.6
	236.7	237.0	0.3	0.1
	295.9	296.0	0.1	0.0
	383.7	384.0	0.3	0.1
Vertical dimensions Za	24.8	25.2	0.5	1.9
	50.6	51.1	0.6	1.1
	75.8	75.0	0.7	1.0
	100.2	99.4	0.7	0.7

whose dimensions were known with an uncertainty of 0.5 m ± 0.2 mm. The target was set in the underwater of 0.15 m in depth. Table 1 shows the comparison between the dimensions estimated by the photogrammetry system and the dimensions measured by rulers. Table 1 suggests the photogrammetry system can determine the horizontal and vertical coordinates with high accuracy. The accuracy of estimating the horizontal coordinates is better than that of estimating the vertical coordinates. The system can estimate the vertical coordinates with an accuracy of better than 1.0 mm. It was found that the system was adaptable to estimating underwater topography of scour around the cylinder with high accuracy.

EXPERIMENTAL RESULTS AND DISCUSSION

(1) Equilibrium scour depth

Figure 2 shows the equilibrium scour depth as function of relative foundation depth *Z/D*. The equilibrium scour depth for a pier with foundation normalized with that for the upper uniform pier S_e/S_{eD} is plotted on the ordinate. Two series' of experimental results obtained by Chabert & Engeldinger (1956) and Melville &

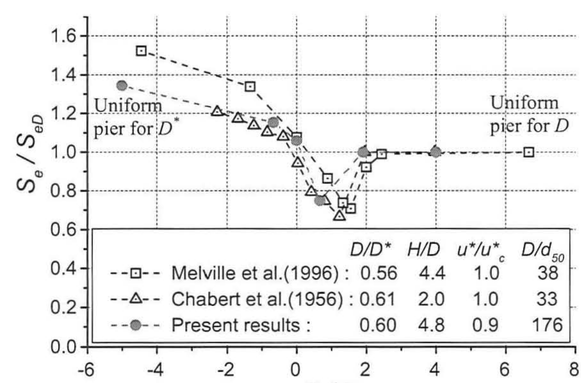

Figure 2. Equilibrium scour depth normalized with that of the uniform pier as function of relative foundation depth.

Raudkivi (1996) for the threshold condition between clear water scour and live bed scour are also included in Figure 2 for comparison with the results of this study. Although there are some differences in experimental conditions as shown in Figure 2, the trend in the three data series is similar. When the foundation depth is larger than the scour depth for the upper uniform pier ($Z/D > S_{eD}/D \approx 1.9$ - 2.4 for these case), the scour depth is the same as that for the uniform pier. The scour depth decreases with decreasing foundation depth when the foundation depth becomes less than the scour depth for the uniform pier. The reduction in scour depth due to the presence of the foundation reaches a maximum when the foundation depth is comparable with the diameter of the upper pier (Z/D = 1 - 1.5). Thereafter, the scour depth increases with decreasing foundation depth. As the foundation protrudes above the initial bed level ($Z/D < 0$), the scour depth increases and approaches that for the downward uniform pier with D^* in diameter, i.e. the scour depth for the foundation alone.

(2) Time evolution of the scour depth

The time evolution of the scour depth normalized with the pier diameter S/D is shown in Figure 3. The depth was measured at the front edge of the pier, relative to the initial bed level. For Z/D = 0.67, the scour depth rapidly increases to the level of the top of the foundation, staying at that depth until about 5 hours into the experiment. Subsequently, the scour depth increases again, gradually approaching the equilibrium depth. For Z/D = 0, the progress of the scour ahead of the pier is initially prevented due to the presence of the top of the foundation and the scour depth then increases to the equilibrium depth. Although the initial increment of the scour depth for Z/D = -0.67 is between Z/D =0.67 and Z/D = 0, the equilibrium scour depth becomes the largest.

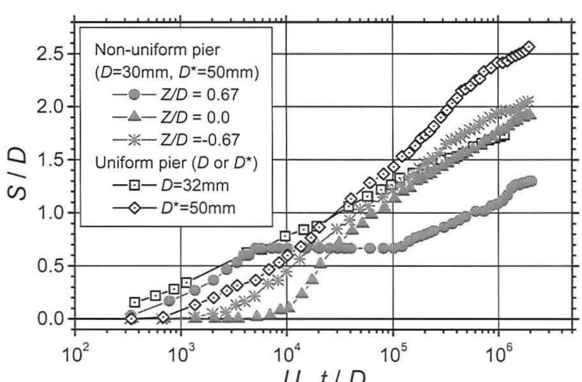

Figure 3. Time variation of scour depths for uniform and non-uniform piers.

(3) Scour topography and sediment transport rate

Figure 4 shows the time evolution of the bed topography during scour development for the pier with foundation of Z/D = 0.67. The negative elevation of

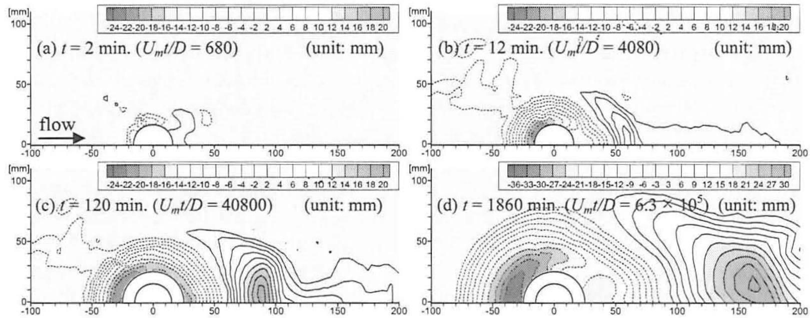

Figure 4. Scour development around the non-uniform pier of Z/D = 0.67.

the scoured bed is denoted by dotted contour lines. The scour process around the pier is in the same way that scour develops around a uniform pier until the foundation expose at the surface of the riverbed (e.g. Umeda et al., 2008). The scour starts at the shoulders of the pier (i.e. 45° from the forward stagnation point), and then the scouring enlarges to the surrounding area along the surface of the pier. Some of the eroded sediment drifts downstream, resulting in deposition of the sediment behind the pier base. As the scour progresses to the level of the top of the foundation, the development of the scour depth is limited and the scour hole formed around the pier keeps on expanding to the horizontal directions. This is mainly because the horseshoe vortex in front of the pier and the shedding vortices behind the pier continue to lift sediment, which is supplied by the sliding of sediment on the slope of the scour hole. Subsequently, the scour reaches the rim of the foundation and the scour depth increases again due to the effect of the horseshoe vortex and the wake vortices. The scour hole around the pier with foundation becomes an inverse truncated cone in shape and the shape of the scour hole is maintained during further scour development (Figure 4 (b)-(d)). The mound of the deposited sediment also appears as some part of the eroded sediment is fed into the downstream of the scour hole. The sediment mound moves to downstream and enlarge gradually. The height of the sediment mound is finally comparable with the depth of the scour hole.

Figure 5 shows the net sediment transport rate estimated with variation in the bed elevation for Z/D = 0.67, according to the method supposed by Izumiya and Uchiyama (1992). The sediment transport rate q_i was calculated by using the Helmholtz theorem and the mass balance of the sediment:

$$\frac{\partial z_b}{\partial t} = -\frac{1}{1-n}\frac{\partial q_i}{\partial x_i} \qquad (i = 1, 2)$$

where z_b is the bed level; t is time; n is the porosity of the bed; x_i is the horizontal coordinates. It is well-known that any vector field can be resolved into the sum of an irrotational vector field and a solenoidal vector field (Helmholtz decomposition). The sediment transport rate q_i estimated in this study corresponds to the irrotational component, which directly affects variation in the bed elevation. It is found in the figure 5 that the vectors of the sediment transport rate tend to be diverged from erosion area and converged into deposition area. The magnitude of q_i increases with

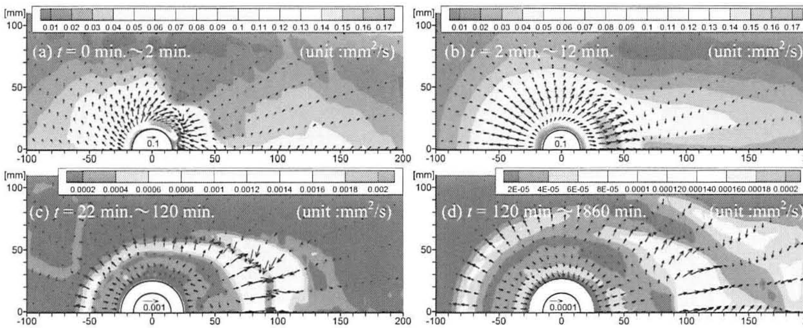

Figure 5. Sediment transport rate estimated with variation in the bed elevation (Z/D = 0.67).

increasing gradient of time-variation in the bed level and tends to be reduced in the scour process. While the sediment transport rate reaches a peak near the side edge of the pier during an initial stage of the scour process (Figure 5 (a)), the location of the peak sediment transport rate shifts to downstream of the pier when the scour hole developed around the pier (Figure 5 (b) and (c)). The sediment transport vectors during the initial stage have a similarity in distribution to the near-bed velocity reported in existing literatures (e.g. Sahin et al., 2007). The distribution of the vectors also consists with the typical motion of the sediment observed in this experiment.

For Z/D = 0.0, where the elevation of the top of the foundation correspond to the initial bed level, the time evolutions of the bed topography and the sediment transport rate are shown in Figure 6 and Figure 7. It is seen that the sediment transport and scour during the initial stage of the scour process are dominant in the wake of the pier. The scour starts in the downstream of the pier and then a pier of depressions is gradually formed in the wake. Some part of the eroded sediment is deposited on the downstream of the depressions. The lee-wake vortices sweep, trap and eject an amount of sediment from the depressions. Most of the sediment ejected by the wake vortices is transported to far downstream of the pier. In contrast, the

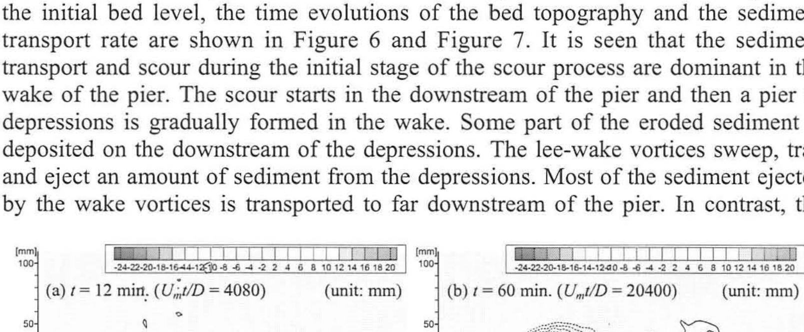

Figure 6. Scour development around the non-uniform pier of Z/D = 0.0.

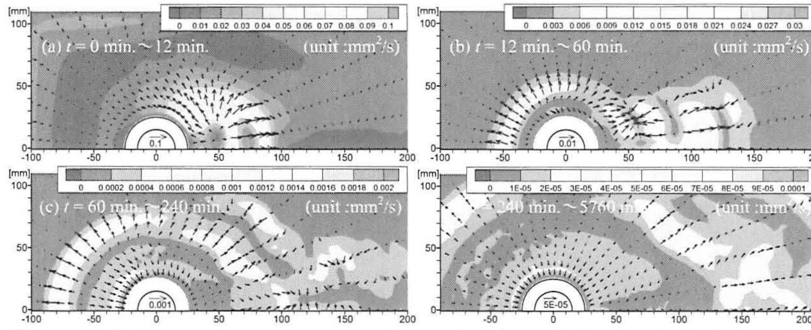

Figure 7. Sediment transport rate estimated with variation in the bed elevation (Z/D = 0.0).

initial progress of the scour upstream of the pier is considerably slower due to the existence of the top of the foundation. The flow accelerated by the contraction of the main flow around the pier starts to sweep the sediment along the rim of the foundation. And then the depressions formed at the shoulders of the foundation gradually enlarge to the surrounding area, resulting in the scour hole being developed.

For Z/D = -0.67, where the top of the foundation is above the initial bed level, the bed topography and the sediment transport rate are shown in Figure 8 and Figure 9. The scour starts at the shoulders of the foundation, and then the scouring enlarges to the surrounding area along the rim of the foundation. Some of the eroded sediment drifts downstream, resulting in the sand ripples being developed on the downstream of the foundation (Figure 8 (a)). As the sand bed ahead of the foundation is eroded to a certain depth, the horseshoe vortex develops in the scour hole formed around the foundation. Since the horseshoe vortex in front of the foundation lifts volumes of the sediment from the scour hole, the scour hole rapidly increases in size and in depth during the middle stage of the scour process (Figure 8 (b)). It is found that the net sediment transport rate q_i increases around the brim of the scour hole (Figure 9 (b) and (c)). There is some part of the eroded sediment swept downstream as bed-load

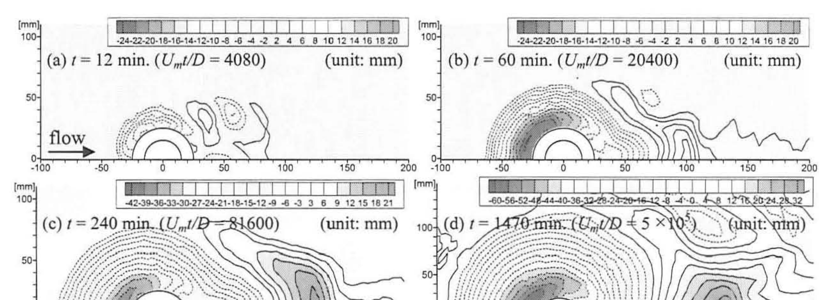

Figure 8. Scour development around the non-uniform pier of Z/D = -0.67.

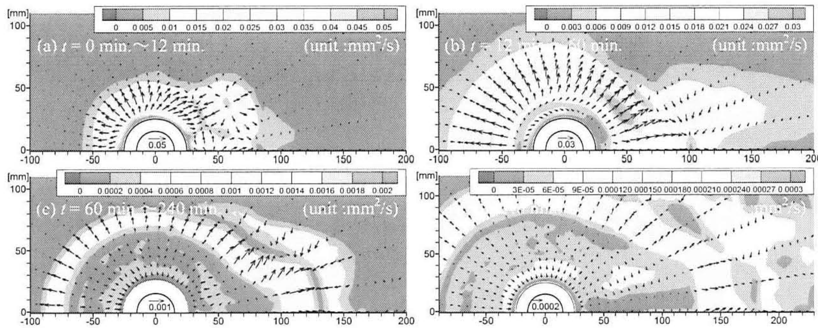

Figure 9. Sediment transport rate estimated with variation in the bed elevation (Z/D = -0.67).

due to the contraction of the flow near the downstream slope of the scour hole. The bed-load leads to formation of the sediment mound downstream of the scour hole. While the initial and middle scour is mainly induced by the flow contraction and the horseshoe vortex respectively, the vortex shedding in the wake also plays an important role in the development of the scour hole as the scour progresses. The wake vortices continue to eject volumes of the sediment from the downstream part of the scour hole. The sediment is transported downstream as suspended-load, which is convected and diffused by time-dependent flow in the wake. As the scour approaches equilibrium stage, the bed-load disappears first and the suspended-load induced by the horseshoe vortex then disappears. The suspended sediment transport by the wake vortices was kept in the experiment.

(4) Volumes of erosion and deposition

Figure 10 shows the time evolutions of the erosion and deposition volumes of the sediment around the piers of Z/D = 0.67, 0.0 and -0.67. The volumes are normalized with the cube of the pier diameter. The erosion and deposition volumes correspond to the volume of the near-pier scour hole V_e and the volume of the prime sediment mound behind the scour hole V_d respectively. The negative volume means erosion. Like the scour depths, the volumes increase with time, but the rates of increase gradually decrease. The deposition volume early achieves an equilibrium value in comparison with the erosion volume. The erosion volume is influenced by the relative foundation depth Z/D. For these cases, the erosion volumes V_e increase with decreasing Z/D. While the normalized erosion volume V_e/D^3 for Z/D = -0.67 reaches about 45 at the end of the test, V_e/D^3 for Z/D = 0.67 is reduced to almost one-half. The influence of the relative foundation depth on the deposition volume of the sediment is not significant in these cases. The maximum volume of the deposition V_d/D^3 is about 10. The sum of the two volumes ($V_t = V_e + V_d$) represents the volume of sediment transported downstream of the deposition mound. While most of V_t can be considered as the suspended-load related to the vortices, most of V_d can be considered as the bed-load related to the contraction of the main flow. It is found in these cases that the ratio of the deposition volume to the erosion volume decreases as

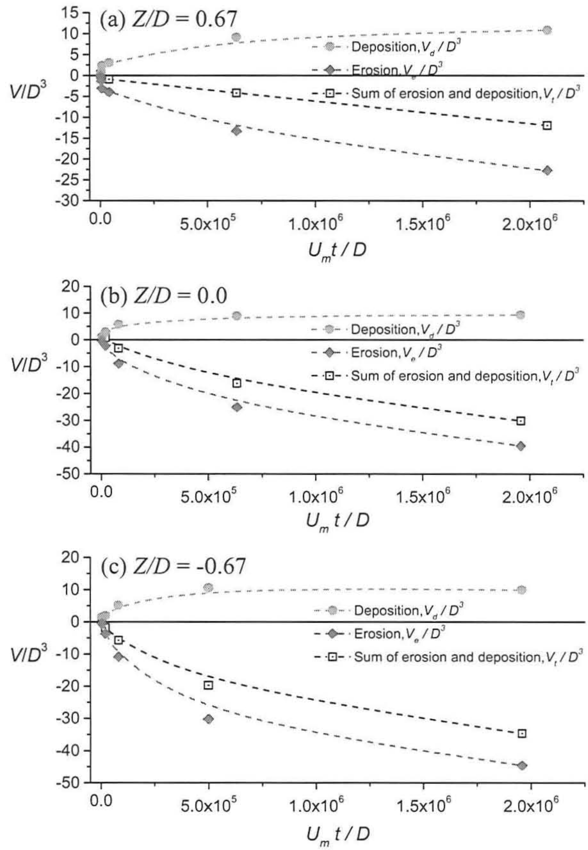

Figure 10. Time variation of the erosion and deposition volumes of the sediment around the piers of *Z/D* = 0.67, 0.0 and -0.67.

scour progresses and tends to increase with increasing *Z/D*. The ratio is calculated in the range of 0.2 to 0.4. It can be seen that the suspended sediment transport becomes more significant as the foundation of the pier protrudes from an initial bed level.

CONCLUSIONS

The following conclusions are based on this experiment on the process of the scour development and sediment transport around a pier with foundation of varying depth from an initial bed level.

The equilibrium scour depth, scour process and sediment transport are influenced by the relative foundation depth *Z/D*. For $S_{eD}/D > Z/D > 0$, the equilibrium scour depth is less than that of a uniform pier S_{eD}. The reduction in scour depth due to the foundation is significant when the foundation depth is comparable with the diameter of the upper pier. For $Z/D = 0$, the scour depth is not very different from S_{eD}. However, the process of the scour development is different from that of a uniform pier. One of the features of the process is that the sediment transport induced by lee-wake vortices is stronger than that by the horseshoe vortex and the contraction of main flow during the initial stage of the scour process. For $Z/D < 0$, the scour depth is larger than that of a uniform pier. The first scour takes place at the shoulders of the foundation and the scouring then enlarges to the surrounding area along the rim of the foundation, resulting in the scour hole being developed.

The influence of Z/D on the deposition volume of the sediment is not significant in these cases. The maximum volume of the deposition is about 10 times the cube of the pier diameter. The erosion volume tends to increase with decreasing Z/D and is estimated in the range of 23 to 45 times.

These experimental results can be useful for understanding of scour mechanism as well as for calibration of a mathematical modeling. However, there is still a great need to obtain understanding of live-bed scouring and scale effects inherent in laboratory flume experiments.

REFERENCES

Chabert, J. and Engeldinger, P. (1956). "Etude des affouilements autour des piles des ponts (Study of scour at bridge piers)." *Rep., Laboratoire National d'Hydraulique*, France.

Izumiya, T. and Uchiyama, T. (1992). "Estimation method of two-dimensional vectors of the sediment transport rate with a potential function for the sediment transport." *Proc. 39th of Coastal Engineering in Japan*, JSCE, vol. 39: 321-325 (in Japanese).

Lu, J.Y., Hong, J.H., Lee, J.J. and Shi, Z.Z. (2008). "Temporal variation of scour depth at nonuniform cylindrical pier with unexposed foundation." *Proc. of 4th Int. Conf. on Scour and Erosion*, (CD-ROM): 174-179.

Melville, B.W and Raudkivi, A.J. (1996). "Effects of foundation geometry on bridge pier scour." *J. Hydraulic Engineering*, 122(4): 203-209.

Melville, B.W. and Yee, M.C. (1999). "Time scale for local scour at bridge piers." *J. Hydraulic Engineering*, 125(1): 59-65.

Sahin, B., Ozturk, N.A. and Akilli, H. (2007). "Horseshoe vortex system in the vicinity of the vertical cylinder mounted on a flat plate." *Flow Measurement and Instrumentation*, Vol. 18: 57-68.

Tsujimoto, T., Murakami, S., Fukushima, T. and Shibata, R. (1987). "Local scour around bridge piers and its protection works." *Mem. Fac. Technol. Kanazawa Univ.*, Japan, Kanazawa, vol. 20, No.1: 11-21.

Umeda, S., Yamazaki, T. and Ishida, H. (2008). "Time evolution of scour and deposition around a cylindrical pier in steady flow." *Proc. of 4th Int. Conf. on Scour and Erosion*, (CD-ROM): 140-146.

Characteristics of Developing Scour Holes around Two Piers Placed in Transverse Arrangement

Mubeen Beg[1], Associate Professor

[1]Civil Engineering Department, Z.H. College of Engineering and Technology, AMU, Aligarh, 202002, UP, India, PH: (91) 941 2460124; e-mail: raisbeg@hotmail.com

ABSTRACT

Local scour at single pier has been extensively studied by several investigators, but scanty work is available on scour around bridge piers founded in close proximity. The work reported herein is concerned with a carefully controlled extensive experimental study of local scour around a group of two bridge piers placed in transverse direction to the flow at varied pier spacing under steady uniform flow clear water scour conditions at flow intensity equal to 0.95. The objective of present study is to investigate the effect of mutual interference of bridge piers on local scour. The data on temporal scour depth, areal extent of scour and sediment deposition around the piers and scour hole characteristics are collected which may provide very useful information to the bridge engineers. Present study reveals that the piers founded in transverse direction to the flow at close proximity may lead to bridge failure, if pier group effect is ignored and bridge piers are designed merely as an isolated pier.

INTRODUCTION

Local scour at group of bridge piers

In case of scour around group of piers, the presence of piers can generate a complex interaction in the hydrodynamic characteristics of the flow field near the piers themselves and therefore, lead to the occurrence and development of a scour process that is quite different from one which occurs around a single pier.

Local scour around a single bridge pier is affected by a large number of inter-dependant variables. The flow, sediment, pier characteristics and time are the main variables affecting this phenomenon. As a consequence of extensive research by several investigators on the phenomenon of local scour around a single bridge pier, a large number of design relationships have been bequeathed to the bridge designer. Not withstanding this, many bridges still suffer damage by local scour. This is due to more intense complexities due to the mutual interaction of piers group. It indicates that in addition to the variables affecting local scour around a single pier, spacing of piers and pattern of piers' placement in the riverbed also affect the scour depth around group of piers.

Hannah (1978), Elliot, K.R. and Baker, C.J. (1985), El-Taher, R.M. (1984, 85). Breusers and Raudkivi (1991), Vittal *et. al.* (1994), Babaeyan-Koopaei and Valentine (1999) and Mubeen Beg (2008) have made some studies on scour around group of piers.

Mechanism of scour around piers placed in transverse arrangement

The presence of group of piers in the river-bed can generate a complex interaction in the hydrodynamic characteristics of the flow field near the piers themselves and therefore, lead to the occurrence and development of a scour process that is quite different from one which occurs around a single pier.

Tison (1940) carried out a model study to investigate the effect on scour depths caused by variation of spacing of piers placed in side-by-side arrangement. He found a mutual interference on maximum scour depth for $Z_c / b \geq 4.3$, where Z_c / b is the lateral spacing of piers measured from center to center. Dietz (1973) made a study of the angle of attack (θ) on maximum scour depth around laterally separated circular piers. He concluded that scour depth is not influenced by (θ) for $Z_c / b \geq 3$.

(Hannah, 1978) has recognized compressed horseshoe vortices responsible to enhance scour at piers placed at close spacing in lateral arrangement. He observed that when piers were placed transverse to the flow, each was having, except at very close spacing, its own horseshoe vortex. As pile spacing was decreased, the inner arms of the horseshoe vortices were observed to be compressed. This caused velocities within the arms of horseshoe vortices to increase with a consequent increase in scour depths.

It can be concluded that it is well established that mostly, the bridge piers are designed as a single pier. However, in the field a bridge is usually supported on a number of piers. Therefore, if a bridge pier is merely designed as a single pier, it may lead to the bridge failure. In these perspectives, to ensure the stability of the bridge piers, the need of a study on the effect of mutual interference of bridge piers on local scour assumes significance. This experimental study investigates the effect of mutual interference on the characteristics of developing scour holes around two piers placed in transverse arrangement.

EXPERIMENTAL PROGRAMME

A series of experiments was conducted to investigate the effect of mutual interference of bridge piers on local scour for the piers located in a direction transverse to the flow at varying lateral pier spacing.

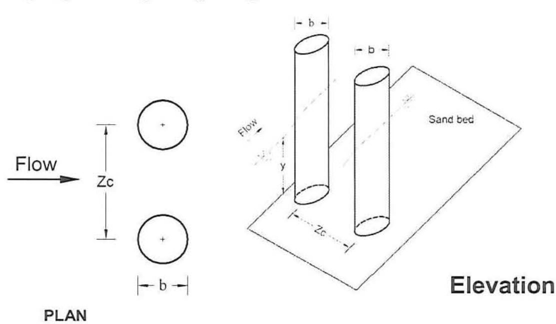

Figure 1. Piers in transverse arrangement

As shown in Figure 1, two circular pier models of 33 mm diameter were set vertically in the sediment bed in the flume at varying lateral spacing, $\frac{Z_c}{b}$ = 1, 2, 3, 4, 5, 6, 7, 8 and 9 where Z_c is the center to center lateral spacing between the piers and b is the pier diameter.

The approach flow was steady uniform for all experiments with average flow depth 140 mm. The stage of particle motion expressed in terms of the shear velocity parameter U_* / U_{*c}, was set so that all the experiments were performed at the clear-water local scour condition $U_* / U_{*c} < 1.0$. The threshold of bed material motion was found by experiment when the pier was not installed. The sediment used in present investigation was cohesionless coarse sand (Median diameter d_{50}=0.95 mm and Geometric standard deviation σ_g=1.187).

Each experiment commenced from a condition of still water at the predetermined flow depth over a leveled bed surface. The time of start of initial movement, and of water surface establishment were recorded. On the completion of the experimental run, the water supply to the flume was gradually stopped and the water from the flume was drained off carefully so that the scour holes and the scour patterns around the piers developed by the flow were not disturbed.

COLLECTION OF DATA AND ANALYSIS OF RESULTS

During the experimental runs, the scour depths were measured at the nose of the two piers at regular interval of time. On the completion of the experimental run, detailed measurements of the scoured area around the piers were made and thereafter the photographs of the scour patterns were taken. The results are analyzed under the following heads:

Variation of scour depth at front faces of piers

During experiments it was observed that both piers scoured to the same depth (± 3mm). Therefore, the maximum scour depths observed at two piers are averaged and plotted against lateral pier spacing 'Z_c/b' as shown in Figure 2.

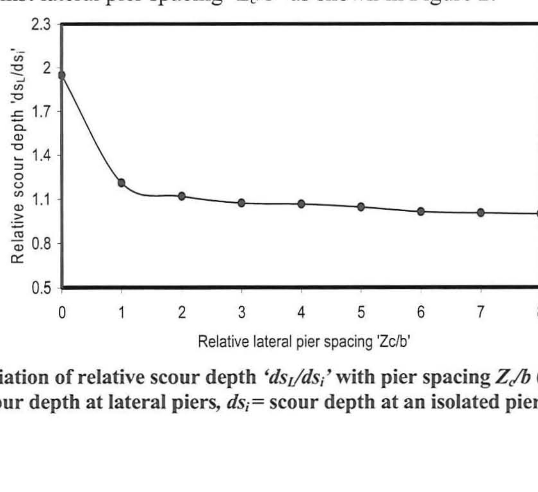

Figure 2.Variation of relative scour depth 'ds_L/ds_i' with pier spacing Z_c/b (where ds_L = scour depth at lateral piers, ds_i= scour depth at an isolated pier).

It is worth mentioning that when the two piers are placed at lateral pier spacing $Z_c/b=0$, the scour depth ds_L is about 1.95 time's ds_i. This is in accordance with the concept of scour depth being proportional to the frontal width of the pier. The scour depth reduces rapidly with piers separation and reaches to about 1.21 (*i.e.*, 'ds_L' about 21% more than 'ds_i') at lateral pier spacing $Z_c/b=1$. The reason for this scour depth being more at $Z_c/b=1$ is the increase in the strength of horseshoe vortex caused by the compression of inner limbs of horseshoe vortices between the two piers. As the pier spacing Z_c/b increases, the effect of compression of horseshoe vortices reduces. Thereafter, the scour depth reduces gradually and reaches to that of an isolated pier at lateral pier spacing $Z_c/b=8$.

Characteristics of scour hole

It was experimentally observed that the flow accelerated between the piers placed at right angles to flow at shorter pier spacings 'Z_c/b' which resulted in an increase in the strength of horseshoe vortices at two piers. As a result, the scour depth increased for same flow, sediment and pier conditions. The characteristics of scour hole vary with the variation in lateral pier spacing 'Z_c/b'. The analysis of important characteristics of scour holes like, length and slope of scour holes at the upstream and downstream face of piers, length of sediment deposition at downstream face of piers, width of scour holes and areal extent of scour are discussed in the following sections.

Since the knowledge of scour hole dimensions is imperative in determining the extent of countermeasures needed to prevent/control scour at piers, various parameters explained as under using present experimental data are determined.

(a) Length of scour hole at upstream faces of piers

The relative lengths of scour hole at upstream face of piers '$L_{shu(L)}/L_{shu(i)}$' are plotted against lateral pier spacing 'Z_c/b' as shown in Figure 3.

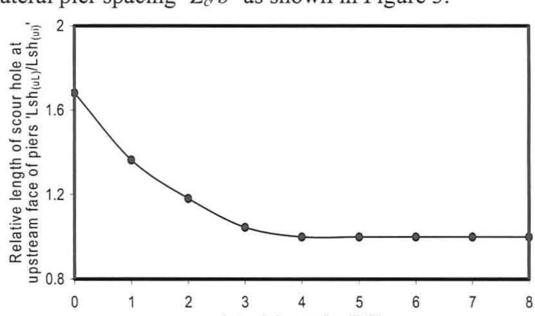

Figure 3. Variation of relative length of scour holes at upstream '$L_{shu(l)}/L_{shu(i)}$' with pier spacing 'Z_c/b'(where $L_{shu(L)}$ = length of scour hole at upstream face of lateral piers , $L_{shu(i)}$ = length of scour hole at upstream face of an isolated pier).

It is observed that the length of scour hole *'$L_{shu(L)}$'* at Z_c/b=0, is about 1.68 times more, than at an isolated pier. This increment occurs due to more frontal width of piers at Z_c/b=0. As the pier spacing Z_c/b increases, frontal width decreases due to gap created between two piers as a result of which *'$L_{sh\ u(L)}/L_{shu(i)}$'* decreases and a decrement of about 63.6 % is noticed at Z_c/b=3. Thereafter, a gradual decrease in the length of scour hole *'$L_{shu(L)}/L_{shu(i)}$'* is observed. This decrease is caused due to the reduction in the effect of compression of horseshoe vortices at piers with increasing pier spacing Z_c/b. The values of *'$L_{shu(L)}/L_{shu(i)}$'* gradually reaches close to unity at Z_c/b=8, which indicates the disappearance of effect of mutual interference between the piers.

(b) Length of scour hole at downstream faces of piers

The relative length of scour holes at the upstream face of piers '$L_{shd(l)}/L_{shd(i)}$' are plotted against lateral pier spacing *'Z_c/b'* as shown in Figure 4.

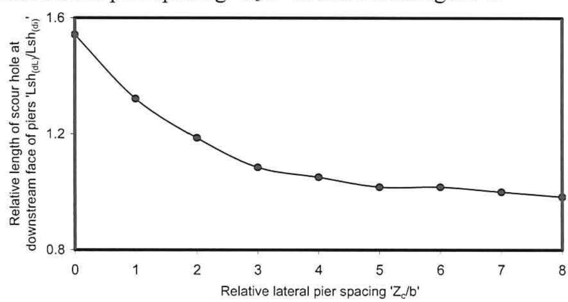

Figure 4. Variation of relative length of scour holes at downstream faces of piers *'$L_{shd(l)}/L_{shd(i)}$'* with pier spacing *'Z_c/b'* (where $L_{shd(l)}$ = length of scour hole at downstream face of lateral piers, $L_{shd(i)}$ = length of scour hole at downstream face of an isolated pier).

Figure 4 reveals that the length of scour hole *'$L_{shd(L)}$'* at pier spacing Z_c/b=0, is about 1.51 times more than what is observed at an isolated pier. This increment in the value of *'$L_{shd(L)}/L_{shd(i)}$'* occurs due to more frontal width of piers at Z_c/b=0. As the pier spacing Z_c/b increases, separation of piers causes a decrease in the value of *'$L_{shd(L)}/L_{shd(i)}$'* and a decrement of about 42.6% in the value of *'$L_{shd(L)}/L_{shd(i)}$'* is noticed at pier spacing Z_c/b=3. Further increase in pier spacing Z_c/b causes a reduction in the effect of compression of horseshoe vortices between the two piers which consequently causes a decrease in the value of *'$L_{shd(L)}/L_{sh\ d(i)}$'*. At pier spacing Z_c/b=8, the value of *'$L_{shd(L)}/L_{shd(i)}$'* approaches to unity which suggests the disappearance of the effect of compression of horseshoe vortices between the two piers.

(c) Slope of scour holes

(i) Slope of scour holes at upstream faces of piers

The relative slopes of scour holes observed at the upstream face of two piers *'$S_{lu(L)}/S_{lu(i)}$'* are plotted against lateral pier spacing *'Z_c/b'* as shown in Figure 5.

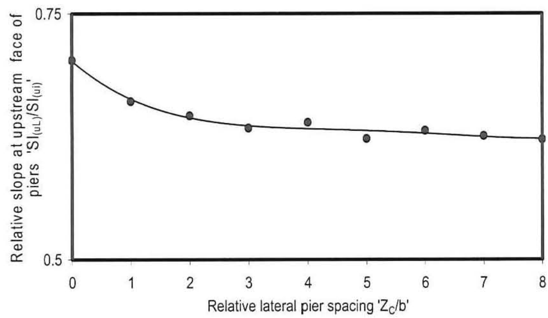

Figure 5. Variation of relative slopes of scour holes at upstream face of piers '$S_{lu(l)}/S_{lu(i)}$' with pier spacing 'Z_c/b' (where $S_{lu(l)}$ = slope of scour hole at upstream face of lateral piers, $S_{lu(i)}$ = slope of scour hole at upstream face of an isolated pier).

At Z_c/b=0, frontal width of piers is more, therefore, the size of scour hole is more, however, increase in length of scour hole is not proportional to the increase in the scour depth. As a result, higher value of '$S_{lu(L)}/ S_{lu(i)}$' can be seen in Figure 5 at Z_c/b =0. As the pier spacing Z_c/b increases, frontal width decreases due to separation of piers. With further increase in pier spacing Z_c/b, the slope '$S_{lu(L)}/S_{lu(i)}$' approaches to unity which is a pointer towards the state of two piers being free from mutual interference.

(ii) Slope of scour holes at downstream faces of piers

Figure 6 shows the relative slope of scour holes at the downstream face of two piers '$S_{ld(L)}/S_{ld(i)}$' with respect to the lateral pier spacing 'Z_c/b'.

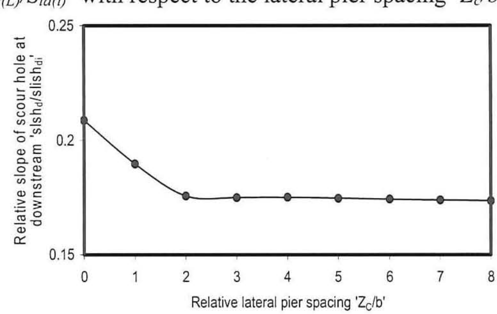

Figure 6. Variation of relative slopes of scour holes at downstream face of piers '$S_{ld(L)}/S_{lu(i)}$' with pier spacing Z_c/b (where $S_{ld(L)}$ = slope of scour hole at downstream face of lateral piers, $S_{ld(i)}$ = slope of scour hole at downstream face of an isolated pier).

At shorter Z_c/b, inner arms of horseshoe vortices at downstream faces of two piers are compressed as a result of which the flow is accelerated between the piers and causes increased scour depths to occur, however, as shown in Figures 2 and 4, this increment in scour depth is not in proportion to the increase in the length of scour hole. Consequently, increased values of '$S_{ld(L)}/S_{ld(i)}$'at pier spacing $Z_c/b=2$ are resulted. However, as noticed in Figure 6, at pier spacings $Z_c/b \geq 2$, the of slope of scour holes at the downstream face of piers is close to that observed at an isolated pier which indicates the diminishing state of mutual interference effect of piers.

(d) Variation of area of scour extents with pier spacing

The areal extents of scour around the piers are plotted for typical pier spacings 'Z_c/b' and shown in Figures 7 and 8 respectively. It can be seen in Figure 7 that the areal extent of scour around the two piers overlap each other upto pier spacing $Z_c/b=6$.

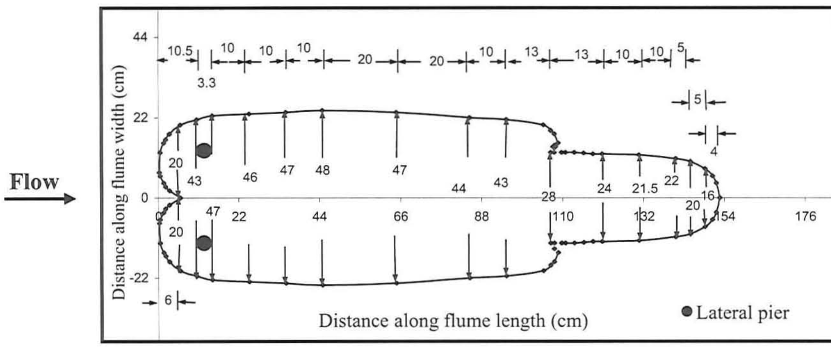

Figure 7. Areal extent of scour around the piers placed in lateral arrangement at $Z_c/b=6$

However, at pier spacing $Z_c/b=8$, as illustrated in Figure 8, the areal extents of scour get completely separated from each other and become similar in shape and size to that around an isolated pier, demonstrating that the two piers become free of effects of mutual interference.

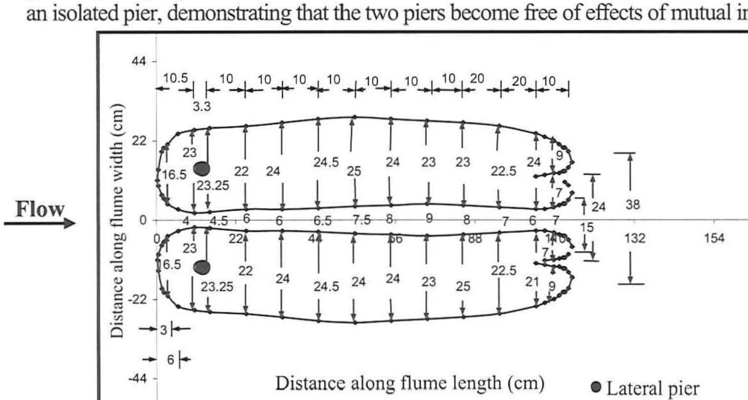

Figure 8. Areal extent of scour around the piers placed in lateral arrangement at $Z_c/b=8$

The areas of scour extents around the piers are divided by twice the area of scour extent estimated for an isolated pier to obtain the relative areas of the scour extent '$A_L/2A_i$' and the same are plotted against lateral pier spacing 'Z_c/b' as shown in Figure 9.

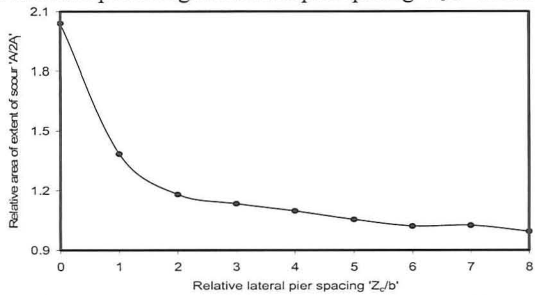

Figure 9. Variation of relative area of scour extent around two piers '$A_L/2A_i$' with pier spacing Z_c/b (where A_L = area of scour extent around the lateral piers, A_i = area of scour extent around an isolated pier).

It is noticed that the value of '$A_L/2A_i$' is maximum at pier spacing Z_c/b=0. This maxima occurs, since, as the frontal width of piers at this pier spacing is twice that of an isolated pier. At Z_c/b=1, a rapid decrease of 65.55 % in the value of '$A_L/2A_i$' is observed.

At pier spacing Z_c/b=1,2,3,4 and 5, the values of areas of scour extent '$A_L/2A_i$' are about 38.5%, 18%, 13.45,10% and 5.4% times more than that at an isolated pier. The values of areas of scour extent '$A_L/2A_i$' gradually decrease and reach close to that at an isolated pier at pier spacing Z_c/b=8. When the pier spacing between two piers Z_c/b increases beyond 1, the flow pattern around two piers become similar to around an isolated pier due to which area of scour extent '$A_L/2A_i$' decreases and approaches to that of an isolated pier.

(e) Width of scour holes

The top width of scour hole of a single pier can be estimated from the relationship of Richardson *et al.* 1993, therefore, top widths 'W_L' are divided by twice the top width of an isolated pier to obtain the relative width $W_L/2W_i$, which are plotted against relative pier spacing Z_c/b as shown in Figure 10.

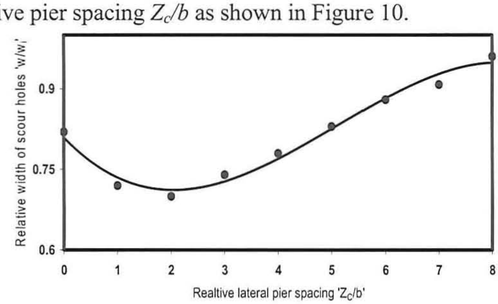

Figure 10. Variation of relative width of scour holes of piers $W_L/2W_i$ with pier spacing Z_C/b. (where W_L = width of scour hole of two lateral pier, W_i = width of isolated pier).

The top width 'W_L' measured at Z_c/b=0 is 1.64 times of top width of a single 'W_i' pier. This increase in width of scour hole is attributed to more frontal width of piers at this pier spacing as the depth of scour and hence the top width of scour hole is directly proportional to the frontal width of pier. When the two piers are separated from one another, the frontal width decreases as a result of which the scour depth decreases and consequently the top width of scour hole decreases. Figure 10shows that the value of '$W_L/2W_i$' reduces to 0.72 at pier spacing Z_c/b=1. However, the value of '$W_L/2W_i$' increases between pier spacings Z_c/b=1 and 8. This increase in the values of '$W_L/2W_i$' is caused due to an increase in pier spacing 'Z_c/b' since the lateral distance between the outer edges of scour extent increases with pier spacing Z_c/b. The value of '$W_L/2W_i$' approaches nearly equal to 0.92 at pier spacing Z_c/b=8, which indicates the diminishing state of mutual interference of piers.

(f) Length of sediment deposition at downstream faces of piers

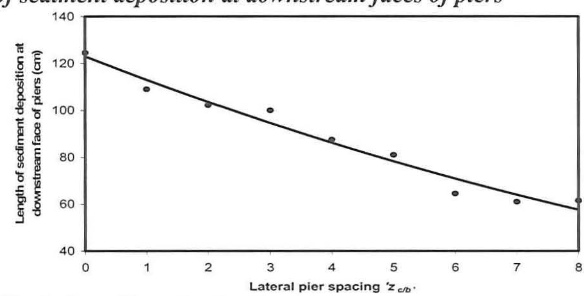

Figure 11. Variation of length of sediment deposition at downstream face of two piers '$L_{dep(l)}$'with pier spacing 'Z_c/b'

The lengths '$L_{dep(L)}$' are divided by the length of sediment deposition '$L_{dep(i)}$' occurring at the downstream face of an isolated pier and the values of relative length of sediment deposition '$L_{dep(L)}/L_{dep(i)}$' are plotted with respect to the pier spacing 'Z_c/b' as shown in Figure 11.

It can be seen that at pier spacing Z_c/b=0, the value of '$L_{dep}/L_{dep(i)}$' is maximum. This maxima is due to the fact that at Z_c/b=0, frontal width of piers is equal to twice the width of an isolated pier. It is also evident that '$L_{dep}/L_{dep(i)}$' decreases with an increase in pier spacing Z_c/b, since, the increment in pier spacing Z_c/b causes decrease in frontal width and thereby a decrease in the length of sediment deposition. At pier spacing Z_c/b=8, the length of sediment deposition approaches to that measured at an isolated pier. Photographs shown in Figure P1 authenticate the interpretation of results on scour characteristics analyzed and discussed above.

CONCLUSIONS

At zero lateral pier spacing, the scour depth is 1.95 times of that occurring at an isolated pier. At lateral pier spacing of one pier diameter, though the scour depth at two piers quickly decreases, nevertheless, it remains 21 % higher than that of an isolated pier. At lateral pier spacing of 8 times the pier diameter, although, the scour depth at two piers becomes same as that of an isolated pier, but the size of the scour holes are not identical to that for an isolated pier. These findings suggest that the two piers should be placed at lateral pier spacing $Z_c/b>8$. According to Raudkivi (1986), the scour depth at five-pier diameter spacing is 1.2 times the local scour at single pier.

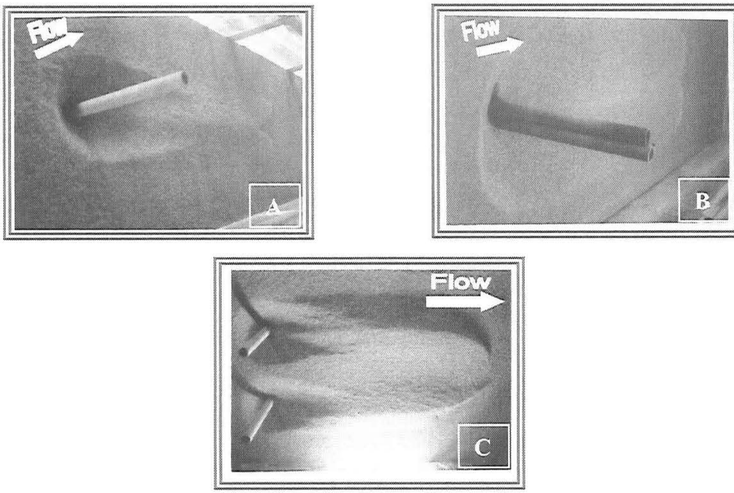

Figure P1. Scour and Deposition Patterns around (A) Single Pier (B) $Z_c/b=0$ (C) $Z_c/b=7$

References

Babaeyan-Koopaei, K. and Valentine, E. M. (1999). Bridge Pier Scour in Self-Formed Laboratory Channels, The XXVIII IAHR Congress, pp. 22-27.

Breusers, H.N.C. And Raudkivi, A.J. (1991). Scouring, Hydraulic Structure Manual, I.A.H.R., Balkema, Rotterdam, Netherlands

Dietz, J.W. (1973). Kalkbildung, An Einem Kreiszylindrischen Pfeilerpaar, Die Bautechnic, 50, pp. 203-208.

Elliot, K.R. And Baker, C.J. (1985). Effect of Pier Spacing on Scour Around Bridge Piers, Journal Of Hydraulics Divn., Proc. ASCE, Vol. 111, No. 7, pp. 1105-1109.

Elliot, K.R. and Baker, C.J. (1985). Effect of pier spacing on scour around bridge piers, Journal of Hydraulics Divn., Proc. ASCE, Vol. 111, No. 7, pp. 1105-1109.

El-Taher, R.M. (1984). Experimental Study on the Interaction between a Pair of Circular Cylinders Normal to a Uniform Shear Flow, J. Wind Eng. Ind. Aerodyn. 17, pp. 117-132.

El-Taher, R.M. (1985). Flow around two parallel circular cylinders in a linear shear flow. J. Wind Engg. Ind. Aerodyn., Vol. 21, pp. 251-272.

Hannah, C.R. (1978). Scour at Pile Groups, University Of Canterbury, N.Z., Civil Engineering Research Rep. No. 78-3, 92.

Mubeen Beg, (2008) Effect of Mutual Interference of Bridge Piers on Local Scour, Ph.D Thesis, Aligarh Muslim University, Aligarh, India.

Richardson *et al.* 1993 Top width of pier scour holes in free and pressure flow. Proc., Nat. Conf. Hydraulic Engrg. Part 1 (of 2) Jul 25-30, pt 1 1993 ASCE p 911.

Tison, L.J. (1940). Scour Around Bridge Piers In Rivers, Annales Des Travaux Publics De Beligique, 41, No. 6,pp. 813-871.

Vittal, N., Kothyari, U.C. And Haghighat, M. (1994). Clear Water Scour Around Bridge Piers Group, J. Hydr. Engrg, ACCE, 120(11), 1309-1318.

Local Scour At Bridge Piers: The Role Of Reynolds Number On Horseshoe Vortex Dynamics

N. Apsilidis[1], S.M. ASCE, P. Diplas[2], M.ASCE, C.L. Dancey[3], P.P. Vlachos[4] and S.G. Raben[5]

[1] Baker Environmental Hydraulics Laboratory, Department of Civil and Environmental Engineering, Virginia Polytechnic Institute and State University, Blacksburg, VA 24061-0105, PH (540) 231-2357, e-mail: napsilid@vt.edu

[2] Baker Environmental Hydraulics Laboratory, Department of Civil and Environmental Engineering, Virginia Polytechnic Institute and State University, Blacksburg, VA 24061-0105, PH (540) 231-6069, e-mail: pdiplas@vt.edu

[3] Baker Environmental Hydraulics Laboratory, Department of Mechanical Engineering, Virginia Polytechnic Institute and State University, Blacksburg, VA 24061-0238, PH (540) 231-7466, e-mail: cld@vt.edu

[4] Advanced Experimental Thermofluid Engineering Research Laboratory, Department of Mechanical Engineering, Virginia Polytechnic Institute and State University, Blacksburg, VA 24061, PH (540) 231-3366, e-mail: pvlachos@vt.edu

[5] Advanced Experimental Thermofluid Engineering Research Laboratory, Department of Mechanical Engineering, Virginia Polytechnic Institute and State University, Blacksburg, VA 24061, PH (540) 231-7187, e-mail: sraben@vt.edu

ABSTRACT

This paper reports a comprehensive study of the major scour agent around bridge piers: the turbulent horseshoe vortex. The intricate and inherently unsteady characteristics of the junction flow are captured within a series of scaled laboratory experiments. We applied the state-of-the art Time-Resolved Digital Particle Image Velocimetry (TR-DPIV) technique to measure the velocity field at the centerline plane of symmetry upstream of a cylindrical model. Three levels of Reynolds numbers (Re_D) based on the obstacle diameter were studied: 26,000, 48,000 and 117,500. We evaluated the effect of this factor based on the time-averaged analyses of velocity and vorticity. Basic statistical analysis of the fluctuating velocity components provided insight to the physical mechanism that governs the behavior of the horseshoe vortex at the aforementioned levels of Re_D.

INTRODUCTION

Erosion of the loose boundary material around bridge piers poses a significant threat to the structural integrity of the bridge. Past studies have identified hydraulic scour as the major cause of bridge failures (Wardhana and Hadipriono, 2003 & Briaud and Hunt, 2006). As a result, a large number of scour-related studies have been documented in the literature (for a comprehensive list, refer to Melville and

Coleman, 2000). Despite the intense research activity, we are still lacking satisfactory answers regarding the dominant characteristics of the scour mechanism.

We put forward that the key in this effort is the study of the intricate system of vortices, which forms at the juncture base and stretches around the obstacle. Named after its shape, the horseshoe vortex is the result of the interaction between the approaching boundary layer and the adverse pressure gradient imposed by the body (Simpson, 2001). In this case, the disturbed flow experiences a three-dimensional separation and the entrained vorticity rolls up to form the vortical system under investigation.

In a pioneering experimental study, Baker (1979) was among the first to evaluate the dynamics of a turbulent boundary layer propagating along a flat plate. His work revealed the topological characteristics of the flow at the upstream centerline plane of symmetry using oil visualizations. In this way, he documented the instantaneous presence of a four-vortex system. Moreover, these experimental data validated the results of dimensional analysis, according to which the position of the main vortex is expressed as a function of the boundary layer displacement thickness δ^* and the Reynolds number based on the body diameter, Re_D. The range of the second parameter was between 4000 and 90,000.

A decade later, another experimental work by Dargahi (1989) enhanced the state of knowledge with velocity measurements collected using a hot-film anemometer. For $20{,}000<Re_D<39{,}000$, a system of at least five vortices was identified. Hydrogen bubble visualizations highlighted the trend for increased flow complexity with Re_D. The existence of a positive relation between the size of vortex system and the Reynolds number was also reported.

Devenport and Simpson (1990) provided a further insight to the physics of the turbulent horseshoe vortex. They applied the high temporal resolution Laser Doppler Anemometry technique using air as the working fluid. Their analysis disclosed the intermittent character of the turbulent flow for Re_D=115,000. Two modes were identified: the backflow and the zero-flow. During the first one, the deflected fluid forms a jet that penetrates the vortex region and propagates toward the upstream. On the other hand, when the zero-flow mode is active, the aforementioned motion is inhibited and finally the jet is ejected upwards. These states were documented in the probability density functions of the streamwise and vertical velocity components, where two distinct peaks were identified. Flow switches between the two modes in a seemingly random manner and this transition is believed to play an important role in the generation of increased turbulent stresses.

Similar findings regarding the quasi-periodic nature of the vortex flow were reported by Agui and Andreopoulos (1992). In this study emphasis was placed on obtaining time-resolved measurements of the wall pressure for two levels of Re_D at 100,000 and 220,000. Their major finding is the existence of bimodal shapes for the root mean square pressure fluctuations in two regions of the flow not previously identified: close to the separation line and in the wake of the cylinder.

Despite the remarkable progress that has been made in the study of the horseshoe vortex dynamics and the unsteady characteristics of junction flows, a comprehensive study that would incorporate the latest advances in experimental fluid mechanics is still lacking. The present work seeks to augment the current state of knowledge about this phenomenon. In order to accomplish our goal, we conducted a series of high spatio-temporal resolution experiments employing the global flow measurement TR-DPIV technique. The investigation was performed for three levels of Re_D corresponding to turbulent junction flows: 26,000, 48000 and 117,500. All measurements reported herein refer to the upstream centerline plane of symmetry.

PHYSICAL MODEL

Experiments were carried out in a recirculating water tunnel. The total length of the channel is 8.74 m, however the test section has dimensions of 1.81 m x 0.61 m x 0.61 m (L x W x H). The bottom and side walls of this section are made of clear acrylic plexiglass to facilitate optical access for the implementation of DPIV technique. Water was initially pumped into a settling chamber, where a set of screens and a 6:1 three-dimensional contraction were used to deliver swirl-free flow.

At the entrance of the test section, we installed a 10 cm wide sand strip so as to trip the flow and bring about the development of a turbulent boundary layer at the location of the cylinder. The data sets were recorded at the junction between the flat bottom and the protuberance at an average distance of 1.55 m from the same reference point.

Three cylindrical PVC pipes of diameters 0.06 m, 0.089 m and 0.168 m were used to generate the horseshoe vortex system for the corresponding levels of Reynolds numbers. Each cylindrical body was mounted vertically on the bottom of the channel (Figure 1).

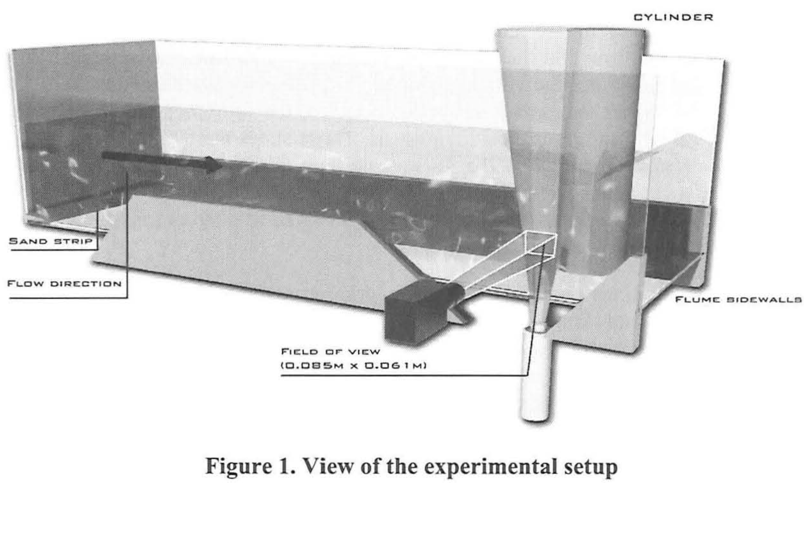

Figure 1. View of the experimental setup

The main factors together with their levels for each experiment are summarized within Table 1.

Table 1. Experimental matrix

Experiment	U(m/s)	H(m)*	D(m)	Fr*	Re_H	Re_D
1	0.40	0.15	0.060	0.33	64,500	26,000
2	0.50	0.18	0.089	0.38	96,770	48,000
3	0.65	0.25	0.168	0.42	174,130	117,500

* H is the flow depth and Fr the Froude number

INSTRUMENTATION

The DPIV system consisted of a double-pulsed Nd: YAG laser source of green wavelength at 532nm. The laser beam was shaped into a planar sheet of approximately 2mm thickness. The light was delivered from the bottom of the flume. Images were taken with an IDT X-3 CMOS high-speed camera. Prior to each data collection session, the optical axis of the camera was carefully aligned until it became perpendicular to the laser plane. To control the operation of the aforementioned pieces of equipment, we connected them to a synchronizer that was monitored through a PC software interface.

Water was seeded with silver-coated hollow glass bead particles with a specific gravity very close to 1 and a mean diameter of 135 um. Given these numbers, the tracers are exhibiting a neutrally buoyant flow behavior. Seeding particles were incrementally introduced into the flow, until we achieved a density of 10-12 particles within an interrogation area of 32x32 pixels.

The magnification factor between the real and the image plane was 63.5 um/pixel. To estimate this value, we took pictures of a steel ruler placed at the centerline of the laser sheet. The physical dimensions of the field of view were 8.5cm x 6.1cm. A total of 3270 images with 1280x1024 pixels resolution were collected at a sampling rate of 1 kHz. The time interval between pulses was 1 ms.

Pre-processing of the PIV data consisted in masking areas of the image that did not include velocity information (solid boundaries). Consequently, we evaluated the raw data by applying a multi-grid, discrete window offset analysis (Westerweel and Dabiri, 1997) in two passes. During the first one, the dimensions of the interrogation window were 64x64 pixels resulting in a grid resolution of 16x16 pixels. In the second pass, the interrogation window was reduced to 32x32 pixels, in order to capture the minute details of the flow. Subsequently, the final grid resolution was increased to 8x8 pixels. In both cases, a Gaussian window was used (Eckstein and Vlachos, 2009) the statistical correlation of image intensities was performed with the Robust Phase Correlation technique (Eckstein et al., 2008). Finally, we validated the flow field applying the Universal Outlier Detector technique of Westerweel and Scarano (2005). In this way, the spurious velocity vectors were identified and substituted with neighboring averages. The final spatial resolution of the velocity field was 0.51 mm and the total number of velocity vectors 20,193.

RESULTS AND DISCUSSION

Time-averaged data analysis

The application of DPIV technique in experimental fluid mechanics yields a vast amount of collected data. Time-averaged analysis provides a concise and efficient way to represent them. For this reason, Figure 2 illustrates contour plots of the streamwise velocity component (expressed in m/s) for each ReD case. The average path of seeding (and consequently fluid) particles is documented by the steamlines of the flow field. To facilitate comparison, the streamwise and vertical dimensions have been normalized with the characteristic length (cylinder diameter).

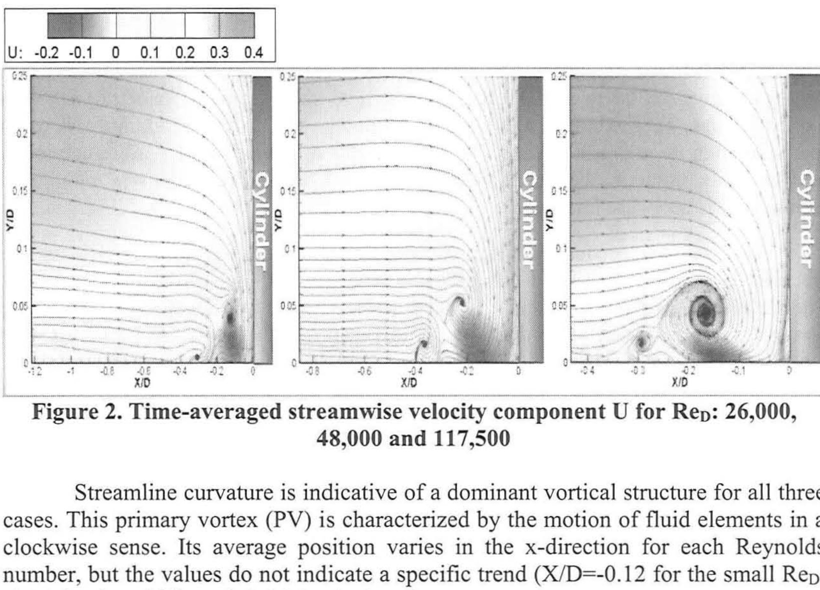

Figure 2. Time-averaged streamwise velocity component U for Re_D: 26,000, 48,000 and 117,500

Streamline curvature is indicative of a dominant vortical structure for all three cases. This primary vortex (PV) is characterized by the motion of fluid elements in a clockwise sense. Its average position varies in the x-direction for each Reynolds number, but the values do not indicate a specific trend (X/D=-0.12 for the small Re_D, -0.21 for the middle and -0.16 for the large).

Moreover, in all cases a secondary vortex (SV) is identified further upstream of the PV. Evidence of a smaller vortex at the corner is provided only for the case of the Re_D=117,500. These results are partially in agreement with the topological analysis of junction flows reported by Hunt et al. (1978). In their study, they propose that a tertiary vortex (TV) forms between the PV and the SV and is rotating in a counter-clockwise sense. Our data do not support the existence of such a vortex with steady space-time characteristics.

Time-averaged, spanwise vorticity contours are displayed in Figure 3 (units are in s^{-1}). Areas of high negative vorticity coincide with high circulation regions that constitute the cores of the PV. Apart from the core vorticity, two distinct vorticity patterns are identified. The first is expressed as a tail of negative vorticity that follows the core. This feature is more prominent for the lowest Re_D, where higher vorticity levels were calculated. The second vorticity pattern is located directly below the PV core. Its existence showcases the interaction between the horseshoe vortex and the solid boundary. Paik et al. (2007) elaborated on the importance of this structure for the eruption of wall vorticity and its contribution to the unsteady nature of the vortex.

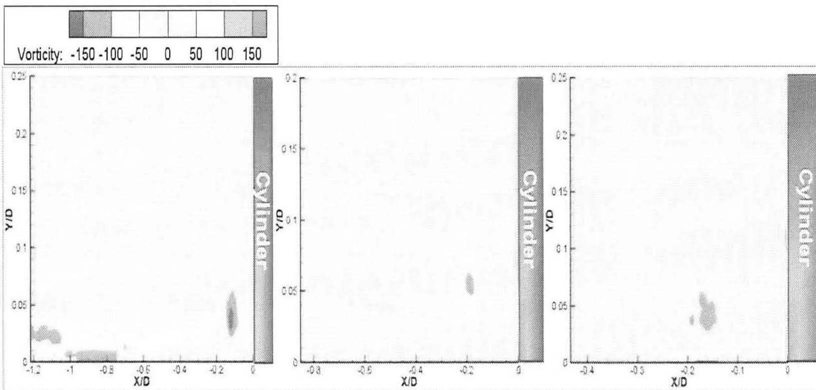

Figure 3. Time-averaged spanwise vorticity for Re_D: 26,000, 48,000 and 117,500

Statistical analysis

Probability density functions (pdf) of both fluctuating velocity components were derived along vertical lines that cross the core of each vortex. Due to the high spatial resolution of DPIV measurements, we were able to reproduce a large number of such plots. However, due to limitations in space, we include here specific cases of the streamwise (u) fluctuations, which are representative of the overall trends. Normalization is performed with the root mean square velocity urms.

The oscillating behavior of horseshoe vortex system between the two modes described in the introductory section is documented with the existence of two peaks. The backflow mode manifests itself by a peak in the area of negative velocities, whereas the zero-flow mode is accompanied with a peak in the positive axis. These characteristics are observed at the region demarcated from the lower streamlines that constitute the PV and the solid boundary. Outside this area, the pdf curves are unimodal.

The aforementioned trend was not observed for the case of the lower Re_D. Figure 4 consists of plots that are characterized by a one-peak distribution. Data are approximately centered around zero. On the other hand, bimodal shapes are present in Figure 5 (corresponding to Re_D=48,000). In this case, the negative peak is greater than the positive one, underscoring the dominance of the backflow state in this continuous interplay of modes. However, the strongest evidence for bimodality is shown in Figure 5. For the highest Reynolds number, the size of the positive peak is comparable to that of the negative one. Therefore, the contribution of the zero-flow mode in the dynamics of high-Reynolds number flows cannot be neglected.

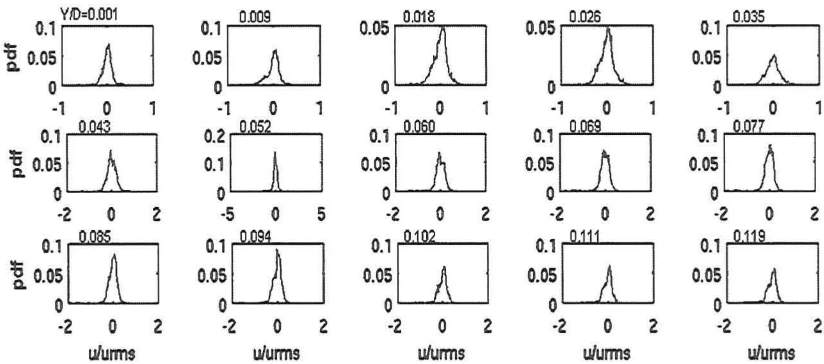

Figure 4. Probability density functions for the u fluctuating component at streamwise location X/D=-0.12 (Re_D=26,000)

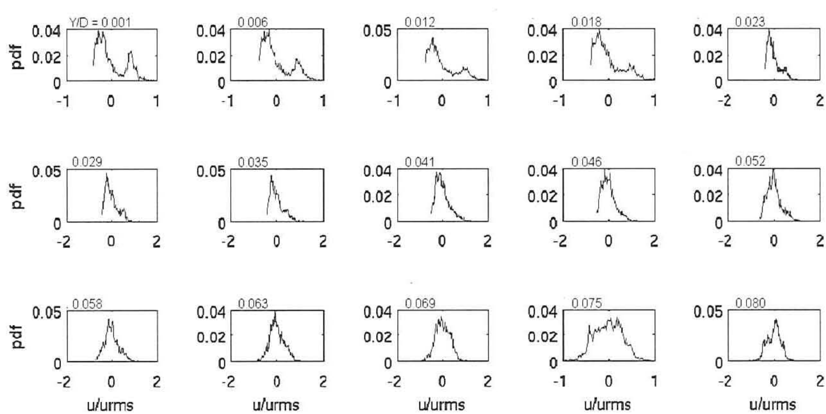

Figure 5. Probability density functions for the u fluctuating component at streamwise location X/D=-0.21 (Re_D=48,000)

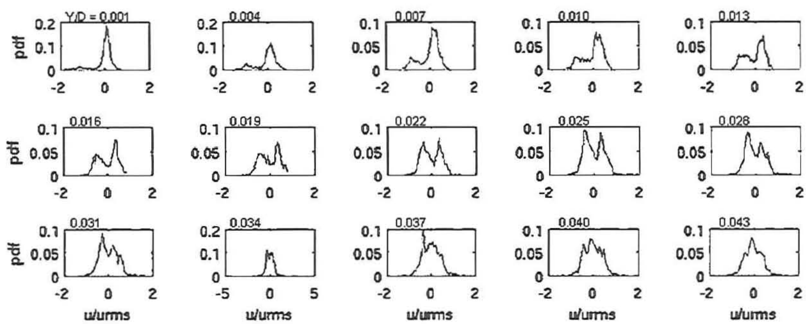

Figure 6. Probability density functions for the u fluctuating component at streamwise location X/D=-0.18 (Re_D=117,500)

CONCLUSIONS

The main purpose of this experimental study was to test the hypothesis that the Reynolds number plays a role in shaping the dynamics of the turbulent horseshoe vortex. Through time-averaged analysis we were able to gain insight into the prevailing characteristics of important flow parameters such as velocity, vorticity and turbulent kinetic energy. As far as the topological characteristics of the flow are concerned, we discovered similarities regarding the structure of the vortex systems. Nevertheless, the distributions of velocity constituents at the region below the horseshoe vortex are revealing that the bi-modal instability is not a universal characteristic of junction flows.

In conclusion, this work adds to the state of knowledge of junction flows in the vicinity of a cylindrical model pier by revealing the dependency of the horseshoe vortex dynamics on Re_D. This finding will guide future experimental work seeking to investigate bridge pier flow characteristics in the presence of a fully-rough, erodible boundary. Sediment transport data will be integrated with time-resolved measurements collected for the present study to validate a numerical model capable of accurately reproducing bridge foundation scour. Once developed, this advanced tool will serve as a valuable resource to engineers toward the safe and financially sound design of bridge foundations.

ACKNOWLEDGEMENTS

Our work was supported by the National Science Foundation (EAR 0738759) and the Research Office of the U.S. Army Corps of Engineers (ARO 53512-EV). The first author would also like to thank the Academy of Athens (Greece) for providing him financial support through the bequest of Praksitelis and Sofia Argyropoulos.

REFERENCES

Agui, J. H., and Andreopoulos, J. (1992). "Experimental investigation of a three-dimensional boundary layer flow in the vicinity of an upright wall mounted cylinder." *Journal of Fluids Engineering* 114: 566-576.

Baker, C. J. (1979). "The turbulent horseshoe vortex." *Journal of Wind Engineering and Industrial Aerodynamics* 6: 9-23.

Briaud, J.L. and Hunt, B.E. (2006). "Bridge scour & the structural engineer." *Structure magazine* 13 (12): 58-61.

Dargahi, B. (1989). "The turbulent-flow field around a circular cylinder." *Experiments in Fluids* 8: 1-12.

Devenport, W. J., and Simpson, R. L. (1990). "Time-dependent and time-averaged turbulence structure near the nose of a wing body junction." *Journal of Fluid Mechanics* 210: 23-55.

Eckstein, A., Charonko, J., and Vlachos, P.P. (2008). "Phase correlation processing for DPIV measurements." *Experiments in Fluids* 45: 485-500.

Eckstein, A., and Vlachos, P. P. (2009). "Assessment of advanced windowing techniques for digital particle image velocimetry (DPIV)." *Measurement Science & Technology*, 20(7): 075402.

Hunt, J.C.R., Abell, C.J., Peterka, J.A., and Woo, H. (1978). "Kinematical studies of the flows around free or surface-mounted obstacles; applying topology to flow visualization." *Journal of Fluid Mechanics* 86: 179-200.

Melville, B.W. and Coleman, S.E. (2000). *Bridge Scour,* Water Resources Publications, Littleton, Colo.

Paik, J., Escauriaza C., and Sotiropoulos, F. (2007). "On the bimodal dynamics of the turbulent horseshoe vortex system in a wing-body junction." *Physics of Fluids* 19(4): 045107.

Simpson, R. L. (2001). "Junction flows." *Annual Review of Fluid Mechanics* (33): 415-443.

Wardhana, K., and Hadipriono, F. C. (2003). "Analysis of recent bridge failures in the United States." *Journal of Performance of Constructed Facilities*, 17(3): 144-150.

Westerweel, J., Dabiri D., and Gharib M. (1997). "The effect of a discrete window offset on the accuracy of cross-correlation analysis of digital PIV recordings." *Experiments in Fluids* 23: 20-28.

Westerweel, J., and Scarano F. (2005). "Universal outlier detection for PIV data." *Experiments in Fluids* 39: 1096-1100.

Trends in Live-Bed Pier Scour at Selected Bridges in South Carolina

Stephen T. Benedict [1] and Andral W. Caldwell [2]

[1]Hydrologist, U.S. Geological Survey, 405 College Avenue, Clemson, SC 29631; email: benedict@usgs.gov
[2]Hydrologist, U.S. Geological Survey, 720 Gracern Road, Columbia, SC 29210; email: acaldwel@usgs.gov

ABSTRACT

The U.S. Geological Survey, in cooperation with the South Carolina Department of Transportation, used ground-penetrating radar to collect measurements of live-bed pier scour at 78 bridges in the Piedmont and Coastal Plain physiographic provinces of South Carolina. The 141 measurements of live-bed pier-scour depth ranged from 0.5 to 5.1 meters. Using hydraulic data estimated with a one-dimensional flow model, predicted live-bed scour depths were computed with scour equations from the Hydraulic Engineering Circular 18 and compared with measured scour. This comparison indicated that predicted pier-scour depths generally exceeded the measured pier-scour depths. At times, predicted pier-scour depths were excessive with overpredictions as large as 7.0 meters. Relations in the live-bed pier-scour data also were investigated, leading to the development of an envelope curve for assessing the upper-bound of live-bed pier scour using pier width as the primary explanatory variable. The envelope curve developed with the field data has limitations, but it can be used as a supplementary tool for assessing the potential for live-bed pier scour in South Carolina. This paper will present findings related to the field investigation of live-bed pier scour. A companion paper presents findings related to live-bed contraction scour that was studied during the same field investigation.

INTRODUCTION

The U.S. Geological Survey (USGS), in cooperation with the South Carolina Department of Transportation (SCDOT), investigated historic scour at 235 bridges in the Piedmont and Coastal Plain physiographic provinces of South Carolina (Benedict, 2003; Benedict and Caldwell, 2006; Benedict and Caldwell, 2009). The general objectives of these studies were to (1) collect field measurements of historic abutment, contraction, and pier scour at sites that could be associated with major floods, (2) use the field data to assess the performance of the scour-prediction equations listed in the Federal Highway Administration Hydraulic Engineering Circular No. 18 (HEC-18) (Richardson and Davis, 2001), and (3) develop regional envelope curves to help assess scour potential in the Piedmont and Coastal Plain regions of South Carolina. The Piedmont and Coastal Plain regions have distinctive hydraulic and soil characteristics that could produce differing scour responses and therefore, the data within these regions were initially evaluated as separate data sets.

These investigations led to the development of a suite of field-derived envelope curves that provide supplementary tools to assist practitioners in South Carolina to assess scour potential for various scour components. Additionally, they have led to the development of large databases that are useful in assessing the general trends of various scour-prediction equations. While there are limitations associated with the South Carolina field data, the large number of data provides a useful means for assessing equation and field trends. The first two field investigations in South Carolina (Benedict, 2003; Benedict and Caldwell, 2006) focused on the occurrence of historic clear-water abutment, contraction, and pier scour on bridge overbanks. Clear-water scour typically occurs on the overbanks of a bridge because upstream floodplain flows do not transport bed sediments into the area of scour. Such conditions provide a readily measured record of historic scour. In contrast, the most recent field investigation (Benedict and Caldwell, 2009) focused on the occurrence of historic live-bed contraction and pier scour. Live-bed scour typically occurs in the main channel at a bridge where bed sediments are transported into the area of scour thus partially or totally refilling the scour holes as flood waters recede. This paper presents findings related to live-bed pier scour. A companion paper presents findings regarding live-bed contraction scour in South Carolina. For expanded details regarding this investigation refer to Benedict and Caldwell (2009).

FIELD DATA

A primary objective of the investigation by Benedict and Caldwell (2009) was to develop a database of live-bed pier-scour field measurements that could be used to assess regional scour trends in South Carolina as well as evaluate the performance of the HEC-18 (Richardson and Davis, 2001) pier-scour equation. When using field data for such purposes, it is important to understand the data characteristics and limitations. Therefore, a brief summary of the field data used in the investigation will be presented.

Live-bed pier-scour holes in South Carolina occur in the main channel of streams and are typically inundated and partially or totally refilled with sediments, making the measurement of these scour holes problematic. Therefore, to measure historic live-bed pier scour under these field conditions, a ground-penetrating radar (GPR) system deployed by boat was utilized. Ground penetrating radar has been used successfully to locate and estimate scour depths associated with historic live-bed scour (Placzek and Haeni, 1995; Webb and others, 2000) and the shallow (6 meters or less) freshwater granular bottom streams of South Carolina provide a favorable environment for the application of GPR. (See Benedict and Caldwell (2009) for details regarding the application and limitations of GPR for the investigation.) To provide some assurance that measured historic scour in this investigation would reflect scour resulting from high flows, USGS streamflow gaging records were reviewed and a strategic set of 78 bridge sites located in the Coastal Plain and Piedmont physiographic provinces of South Carolina were selected for data collection (Figure 1). The set included older bridges that likely had undergone a large flood (the bridge age ranged from 6 to 105 years with a median of 56) and bridges known to have experienced larger floods, with 48 sites having historic floods near to or exceeding the 1-percent exceedance flow. One-hundred and forty-one measurements of historic live-bed pier scour were collected in the investigation with 99 measurements collected in the Coastal Plain with scour depths ranging from 0.5 to 5.1 meters and 42 measurements collected in the Piedmont with scour depths ranging from 0.2 to 0.8 meters. The streams of the Coastal Plain and Piedmont physiographic provinces have regional characteristics, with the Coastal Plain streams tending to

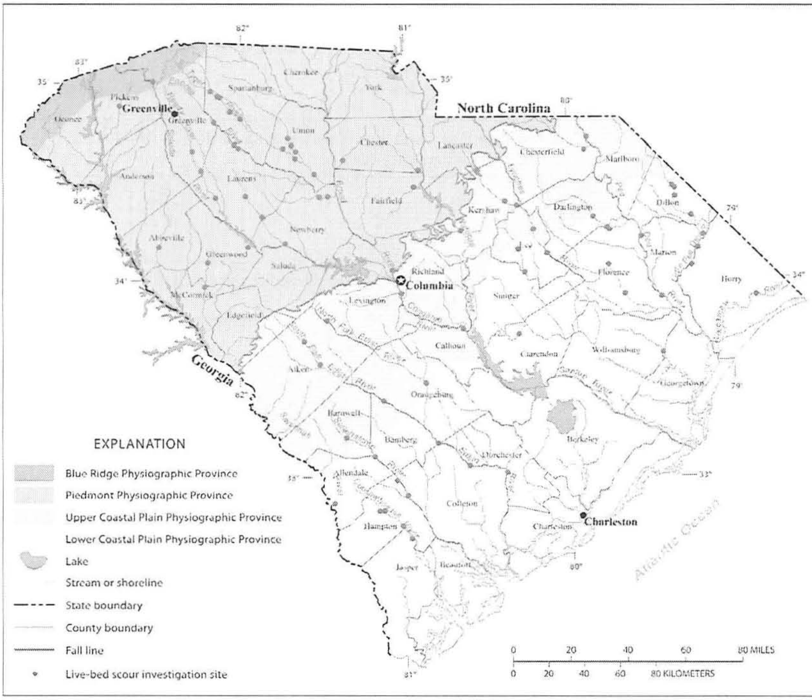

Figure 1. Location of live-bed pier-scour sites in South Carolina.

have lower gradients, lower flow velocities, and longer flood-flow durations in contrast to the Piedmont streams. Table 1 presents the minimum, maximum, and median values of selected stream characteristics in this investigation and highlights the differing stream trends for the two regions. Because of the differing regional characteristics, the Coastal Plain and Piedmont data were initially analyzed as separate data sets to determine if significant regional trends existed. The analysis indicated that the regional distinctions were insignificant and the data for these regions were combined for the development of the South Carolina live-bed pier-scour envelope curve.

To supplement the South Carolina field data, 92 field measurements of live-bed pier scour from the USGS National Bridge Scour Database (NBSD; U.S. Geological Survey, 2001; Table 1) having similar characteristics to the South Carolina data were used. These data included measurements at 16 bridges in 9 States (Alaska, Arkansas, Colorado, Georgia, Indiana, Louisiana, Ohio, Minnesota, and Missouri). Most of the NBSD scour data were collected during high-flow events and measurements of the flow were often taken concurrently with the scour measurements. The supplementary field data only were used to verify trends in the field envelope curves.

Table 1. Range of Selected Parameters for Field Measurements of Pier Scour

Range value	Drainage area (square kilometer)	Channel slope (meters/ meter)	Average approach velocity (meters/ second)	Average approach depth (meters)	Pier width (meters)	Median grain size (milli-meter)	Measured pier-scour depth (meters)
South Carolina Live-Bed Pier-Scour Data -- Piedmont (Benedict and Caldwell, 2009) (42 measurements)							
Minimum	54.4	0.0002	0.5	2.1	0.2	0.5	0.6
Median	383	0.0070	2.2	5.9	1.2	1.0	1.4
Maximum	13,600	0.0016	2.9	8.3	1.8	1.7	2.7
South Carolina Live-Bed Pier-Scour Data -- Coastal Plain (Benedict and Caldwell, 2009) (99 measurements)							
Minimum	44.5	0.0001	0.2	0.9	0.3	0.2	0.5
Median	2,670	0.0003	1.3	4.8	0.5	0.6	1.2
Maximum	24,200	0.0020	2.7	15.5	2.7	1.7	5.1
National Field Data (U.S. Geological Survey, 2001) (92 measurements)							
Minimum	1,200[a]	0.0001[b]	0.3	0.5	0.8	0.1	0.2
Median	95,300	0.0002	1.4	7.7	2.8	0.5	1.4
Maximum	1,800,000	0.0010	3.9	20.0	5.5	1.8	7.7

[a] Drainage areas for 3 of the 16 bridge sites were not available.
[b] Channel slopes for 6 of the 16 bridge sites were not available.

The field measurements used in this investigation provide a large set of historic live-bed pier-scour data offering a valuable resource for gaining insights to scour trends within the field. However, the limitations of these data must be kept in mind when using the data to assess scour trends. Some of these limitations for the South Carolina data include (1) errors associated with GPR measurements and interpretations, (2) field complexities that may limit the ability to properly measure and (or) interpret the scour data, (3) field complexities that may produce scour anomalies, and (4) errors associated with hydraulic estimates from flow models. The noted limitations associated with the South Carolina live-bed pier-scour data will introduce error into the analysis for this investigation, making the data less than ideal. However, the large number of field measurements, in conjunction with the NBSD data, provides a means for evaluating the general trends of live-bed pier scour in South Carolina.

COMPARISON WITH LABORATORY DATA

Figure 2 shows the South Carolina live-bed pier-scour data and the laboratory data used to develop the original HEC-18 pier-scour equation (Richardson and others, 1991) plotted in a dimensionless format. (Note: Field measurements with pier skews were excluded in Figure 2.) The trend line through the laboratory data represents the original HEC-18 pier-scour equation in a power function format. The South Carolina live-bed pier-scour data have a larger scatter than that of the laboratory data; however, the trend line for the field data is similar to that of the laboratory data, indicating that the South Carolina field data are capturing the anticipated trends. This

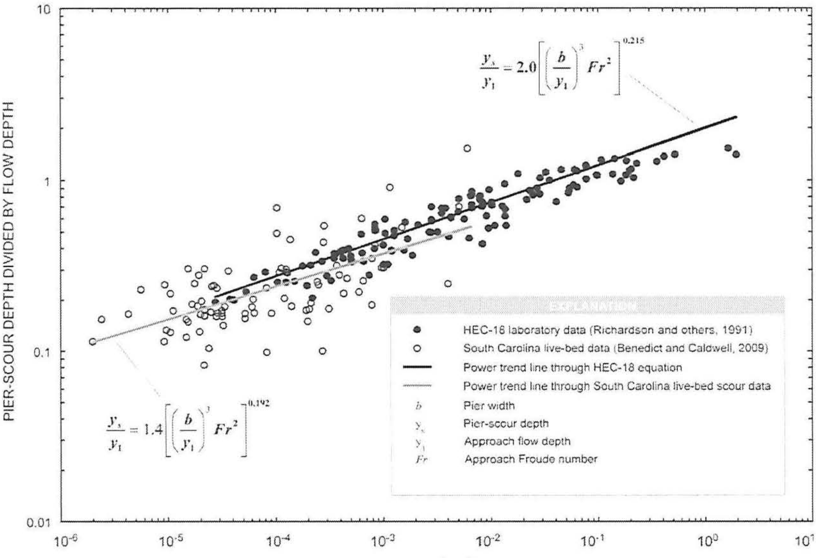

Figure 2. Relation of relative scour (y_s/y_1) to the dimensionless variable, $(b/y_1)^3Fr^2$, for laboratory data used to develop the original HEC-18 pier-scour equation (Richardson and others, 1991) and data from selected sites in South Carolina (from Benedict and Caldwell (2009)).

provides confidence that the South Carolina live-bed pier-scour data are reasonable and therefore can be used to assess the performance of scour-prediction equations to develop regional envelope curves.

EVALUATION OF HEC-18 EQUATION

To predict live-bed pier-scour depth, Richardson and Davis (2001) recommend using the following equation that initially was derived from laboratory data for noncohesive sediments and later was modified with correction coefficients to account for coarse sediments and wide piers.

$$\frac{y_s}{b} = 2.0K_1K_2K_3K_4\left[\frac{y_1}{b}\right]^{0.35} Fr_1^{\ 0.43}, \tag{1}$$

where

y_s is the predicted pier-scour depth, in meters;

b is the pier width, in meters;

K_1 is the dimensionless correction coefficient for pier-nose shape;

K_2 is the dimensionless correction coefficient for flow angle of attack;

K_3 is the dimensionless correction coefficient for streambed conditions;

K_4 is the dimensionless correction coefficient for streambed armoring;

y_1 is the approach-flow depth, in meters; and

Fr_1 is the approach-flow Froude number defined as

$$Fr_1 = V_1 / (gy_1)^{0.5};$$

where

V_1 is the mean approach velocity, in meters per second; and

g is the acceleration of gravity, in meters per square second.

Using hydraulic variables estimated from a one-dimensional model with the estimated historic flows, predicted pier-scour depths were computed using equation 1. Twenty-five of the 141 pier-scour measurements required a complex pier-scour computation as described in HEC-18 (Richardson and Davis, 2001), and at these piers, both the standard (eq. 1) and complex pier-scour computations were made. Predicted pier-scour depths were compared with measured pier-scour depths for the Coastal Plain and Piedmont regions, as shown in Figure 3. Figure 3A shows the results of predicted scour based on the standard pier-scour computation (eq. 1), and Figure 3B includes data from the 25 complex pier computations. The trends of Figure 3A indicate that the standard HEC-18 pier-scour equation (eq. 1) underpredicts approximately 16 percent of the data, with underprediction ranging from 0.03 to 1.0 meter with a median value of 0.2 meter. The frequency of overprediction is approximately 84 percent of the data, with overprediction ranging from 0.03 to 4.1 meters with a median value of 0.6 meter. Benedict and Caldwell (2006) and Mueller and Wagner (2005) noted similar trends for clear-water pier scour in South Carolina and selected data from the NBSD (U.S. Geological Survey, 2001), respectively, with slightly lower rates of underprediction. The higher rate of underprediction for the South Carolina live-bed data can be attributed, in part, to the potential error associated with the GPR data collection and interpretation. Figure 3B includes predicted scour associated with the 25 complex pier-scour computations and indicates that when this procedure is applied to complex piers, it tends to produce larger estimates of scour than the standard equation (eq. 1). Based on the results of Figure 3 and those of Benedict and Caldwell (2006) and Mueller and Wagner (2005), it is reasonable to conclude that using the HEC-18 standard and complex pier-scour equation generally provides conservative estimates of pier scour that, at times, can produce excessive overprediction (as large as 7 meters in Benedict and Caldwell (2009)) with occasional underprediction.

ENVELOPE CURVES

Benedict (2007) provides an overview for the development of regional bridge-scour envelope curves and lists the assumptions and supporting justification on which they are derived. These assumptions include, (1) scour is influenced by the hydrology and geology of a physiographic region, and therefore, will display regional trends, (2) just as there are limits to maximum scour depth within laboratory data there will be limits in field data that can be used to form an upper-bound envelope curve of historic scour, and (3) scour has a strong correlation to geometric variables, such as pier width and the geometric contraction ratio, and these geometric variables

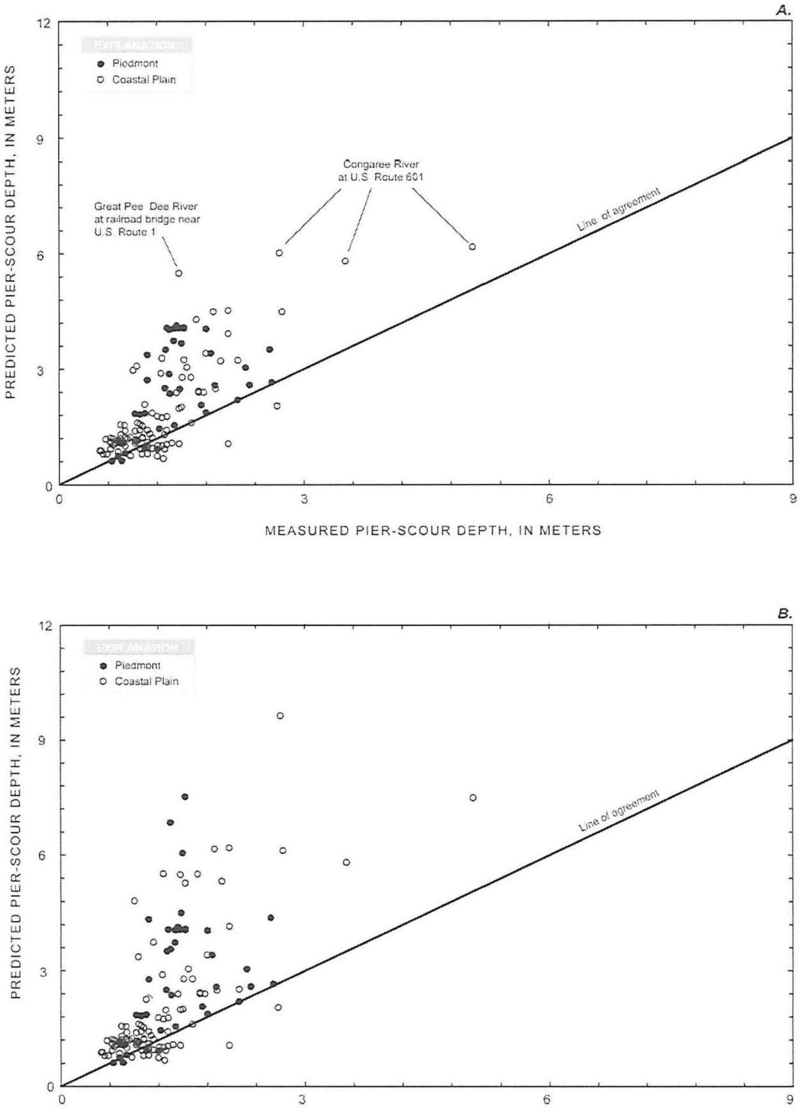

Figure 3. Relation of measured live-bed pier-scour depth to predicted pier-scour depth (A) neglecting the complex pier computation and (B) using the complex pier computation for the maximum historic flows at selected sites in South Carolina (from Benedict and Caldwell (2009)).

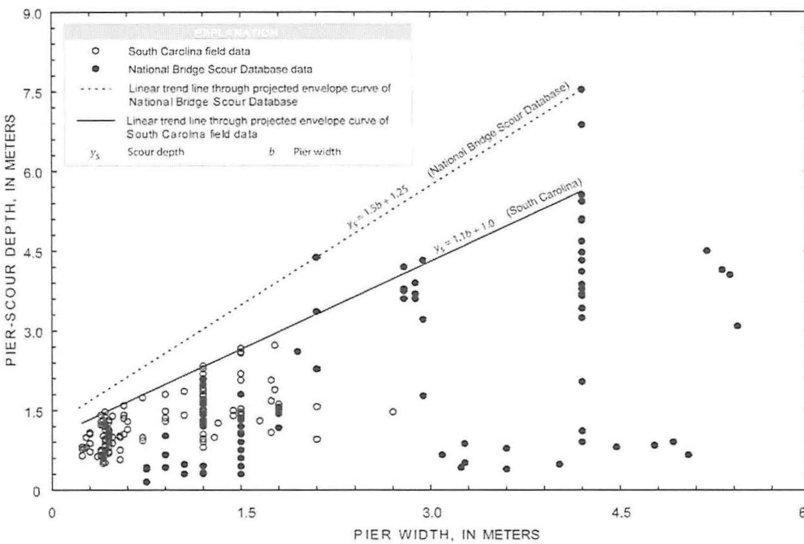

Figure 4. Envelope curves for pier-scour depth for selected field data (modified from Benedict and Caldwell (2009)).

can be used as the explanatory variable to develop simple but useful regional bridge-scour envelope curves. These assumptions formed the foundation for developing the South Carolina live-bed pier-scour envelope curves.

In developing bridge-scour envelope curves, an appropriate geometric variable that is strongly correlated to the scour component of interest must be selected for use as an explanatory variable. In the case of pier scour, scour depth will be strongly correlated to pier width (Laursen and Toch, 1956; Melville and Coleman, 2000; Richardson and Davis, 2001; Mueller and Wagner, 2005). The envelope curves in Figure 4 show the upper-bound trends for the relation of measured pier-scour depth and pier width for the South Carolina and NBSD data. (Note: Field measurements with significant skews were excluded from Figure 4.) The field envelope curves and their associated equations have similar quantitative trends with an increase in the upper bound of scour with increasing pier width. Benedict and Caldwell (2009) compared these field envelope curves with envelope curves for selected laboratory data. While the quantitative values between field and laboratory varied, the qualitative trends were very similar indicating that the trends for the field data are reasonable.

Laboratory investigations note that the system of vortices generated by flow around a pier is the mechanism that produces pier scour. The dominant factors within this system that contribute to scour production are the downflow at the face of the pier and the horseshoe vortex at the base of the pier (Melville and Coleman, 2000). Hydraulic, soil, and geometric characteristics will influence the magnitude of scour produced by the system of vortices, with pier width having a prominent and proportional influence. Therefore, as pier width increases, and other variables remain constant, there will be a proportional increase in scour depth. The patterns displayed by the envelope curves in Figure 4 are consistent with laboratory findings further confirming that the trends for the field data are reasonable.

The majority of the NBSD data falls within, or is very close to, the South Carolina envelope curve. The three measurements that significantly exceed the envelope curve (Figure 4) are associated with large rivers having drainage areas that range from 135,000 to 157,000 square kilometers, which are significantly greater than the basin sizes associated with the South Carolina data where the range is from 44.5 to 24,200 square kilometers and the median size is 653 square kilometers. The larger drainage areas associated with the three NBSD data imply larger and more complex river channels that could increase the potential for turbulence and secondary flow patterns which could possibly increase scour potential. Additionally, these data points are associated with larger pier widths having complex pier foundations and the limited notes in the NBSD suggest that the pier footings were possibly exposed at the time of the scour measurement, thus potentially increasing the pier-scour depth. The limited notes also indicate that these piers were located in zones of contraction scour suggesting that the measured scour may be influenced by contraction scour in addition to local pier scour. While the field notes are inconclusive, they suggest some possible explanation of why these 3 data points exceed the South Carolina data.

The envelope curve for the South Carolina data in Figure 4 provides a useful supplementary tool for evaluating the potential for live-bed pier scour in South Carolina. For a more conservative evaluation of scour, the envelope curve for the NBSD data can be used. However, the limitations and uncertainty associated with the data used to develop these envelope curves will introduce some uncertainty. Therefore, caution and judgment must be used when applying them. Benedict and Caldwell (2009) provide additional information on the envelope curves regarding their development, limitations, and application.

CONCLUSIONS

A GPR system can be a useful tool to measure historic live-bed scour depths within stream channels. Data from such a system can be used to approximate the regional range and trend for scour that can be used for developing regional bridge-scour envelope curves. For the case of live-bed pier scour, the South Carolina data show similar trends to laboratory and other field data indicating that the South Carolina data are reasonable and can be used to assess the performance of scour-prediction equations to develop regional envelope curves. These envelopes can help engineers assess the reasonableness of predicted scour and the potential for scour within a region of interest. Historic scour data measured with a GPR system will always have error and uncertainty associated with them, and this should be kept in mind when using these data to assess historic scour patterns. Additional information regarding the development, limitations, and application of the envelope curves can be found in Benedict and Caldwell (2009).

REFERENCES

Benedict, S.T. (2003). Clear-water abutment and contraction scour in the Coastal Plain and Piedmont Provinces of South Carolina, 1996-99. U.S. Geological Survey Water-Resources Investigations Report 03-4064, 137 p.

Benedict, S.T. (2007). "Development of regional envelope curves for assessing limits and trends in scour." *Proceedings of The 2007 World Environmental and Water Resources Congress*, Tampa, Florida, (CD-ROM) American Society of Civil Engineers, Reston, Virginia.

Benedict, S.T., and Caldwell, A.W. (2006). Development and evaluation of clear-water pier and contraction scour envelope curves in the Coastal Plain and Piedmont of South Carolina. U.S. Geological Survey Scientific Investigations Report 2005–5289, 98 p.

Benedict, S.T. and Caldwell, A.W. (2009). Development and evaluation of live-bed pier and contraction scour envelope curves in the Coastal Plain and Piedmont provinces of South Carolina. U.S. Geological Survey Scientific Investigations Report 2009-5099, 108 p.

Laursen, E.M., and Toch, A. (1956). Scour around bridge piers and abutments. Iowa Highway Research Board, Bulletin No. 4, 60 p.

Melville, B.W. and Coleman, S.E. (2000). Bridge Scour. Highlands, Colorado, Water Resources Publications, LLC, 550 p.

Mueller, D.S., and Wagner, C.R. (2005). Field observations and evaluations of streambed scour at bridges. Federal Highway Administration, Publication FHWA-RD-03-052, 122 p.

Placzek, Gary, and Haeni, F.P. (1995). Surface-geophysical techniques used to detect existing and infilled scour holes near bridge piers. U.S. Geological Survey, Water-Resources Investigations Report 95-4009, 44 p.

Richardson, E.V., and Davis, S.R. (2001). Evaluating scour at bridges. Federal Highway Administration Hydraulic Engineering Circular No. 18, Publication FHWA-NHI-01-001, 378 p.

U.S. Geological Survey. (2001). National Bridge Scour Database, accessed October 15, 2008, at http://water.usgs.gov/osw/techniques/bs/BSDMS/index.htm

Wagner, C.R., Mueller, D.S., Parola, A.C., Hagerty, D.J., and Benedict, S.T. (2006) "Scour at contracted bridges." *Transportation Research Board.* National Cooperative Highway Research Program Document 83 (Project 24-14), 299 p., accessed December 19, 2008, at http://onlinepubs.trb.org/onlinepubs/nchrp/nchrp_w83.pdf

Webb, D.J., Anderson N.L., Newton T., and Cardimona S. (2000). "Bridge scour: Application of ground penetrating radar." Federal Highway Administration and Missouri Department of Transportation special publication. (http://utc.mst.edu/documents/scour.pdf accessed March 2, 2010).

Time-Dependent Scour Depth under Bridge-Submerged Flow

J. Guo[1], K. Kerenyi[2], H. Shan[1], Z. Xie[1], Y. Zhai[1], and L. Zhao[1]

[1]Dept. of Civil Engineering, University of Nebraska-Lincoln, PKI 204D, 1110 67th ST, Omaha, NE 68182; PH (402)-554-3873; email: jguo2@unl.edu
[2]Office of Infrastructure R&D, Turner-Fairbank Highway Research Center, Federal Highway Administration, 6300 Georgetown Pike, McLean, VA 22101.

ABSTRACT

Current practice for determining the scour depth at a bridge crossing is based on the equilibrium scour depth of a design flood (e.g., 50-year, 100-year, and 500-year flood events), which is unnecessarily larger than a real maximum scour depth during a bridge life span since the peak flow period of a flood event is often much shorter than the corresponding scour equilibrium time. The objective of this study was to present a design method for time-dependent scour depth under bridge-submerged flow. To this end, a series of flume experiments on scour depth under bridge-submerged flow were conducted to collect scour data at different times. A semi-empirical model for estimating time-dependent scour depth was then presented based on the mass conservation of sediment, which agrees very well with the collected data. The proposed method can appropriately reduce the design depth of bridge scour according to design flow and a peak flow period, which can translate into significant savings in the construction of bridge foundations.

INTRODUCTION

Equilibrium scour depth under bridge-submerged flow at clear water threshold condition has been studied by Arneson and Abt (1998), Umbrell et al. (1998), Lyn (2008), and Guo et al. (2009). These studies showed that equilibrium conditions are attained under very long flow durations. In other words, the use of an equilibrium scour depth leads to overly conservative scour depth estimates that translate into excessive costs in the construction of bridge foundations. To improve the cost-efficiency of bridge foundation designs or retrofits, the time-dependent scour depth under bridge-submerged flow is of practical relevance.

The study of time-dependent scour depth has been reported extensively in literature, but all of them were under free surface flow condition about pier scour (Dargahi 1990, Yanmaz and Alitmbilek 1991, Melville 1992, Kothyari et al. 1992, Melville and Chiew 1999, Chang 2004, Oliveto and Hager 2005, Lopez et al. 2006, Yanmaz 2006, Lai et al. 2009) and abutment scour (Oliveto and Hager 2002, Coleman et al. 2003, Dey and Barbhuiya 2005, Yanmaz and Kose 2009). None of them were about general scour under bridge-submerged flow condition. The objective of this study was then to develop a semi-empirical model for computing the time-dependent variation of the maximum clear-water scour depth under bridge-submerged flow. To this end, a series of flume tests were, first, conducted to collect time-dependent scour data. A semi-empirical model was, next, developed based on the conservation of mass for sediment. The proposed model was, then, tested by the collected data. Finally, an implication and limitation was noted for guiding practical applications and further researches.

EXPERIMENTAL STUDY

The experimental study was aimed at understanding the time-dependent scour processes in bridge-submerged flow and collecting data for the development of a semi-empirical model for scour depth. The experiments were performed in the FHWA J. Sterling Jones Hydraulics Laboratory, located at the Turner-Fairbank Highway Research Center in McLean, VA. The experimental setup, results and discussion are described in the following subsections.

Experimental Setup

The experimental setup was the same as that in Guo et al. (2009). The flume had a length of 21.35 m, width of 1.83 m, and depth of 0.55 m, with clear sides and a stainless steel bottom that was about horizontal, where although a uniform flow could not be formed in the flume, it does not affect the results significantly since bridge-submerged flows are rapidly varied, the effect of bottom slopes can be neglected. In the middle of the flume was installed a test section that consists of a narrowed channel with length of 3.04 m and width of 0.63 m, a 40-cm sediment recess, and a model bridge above the recess. A honeycomb flow straightener and a trumpet-shaped inlet were carefully designed to smoothly guide the flow into the test channel. The water in the flume was supplied by a circulation system with a sump of 210 m^3 and a pump with capacity of 0.3 m^3/s; the depth of flow was controlled by a tailgate; and the experimental discharges were controlled by a LabView program and checked by an electromagnetic flowmeter.

During the experiments, two uniform sands (the gradation coefficient $\sigma_g < 1.5$) were used: a median diameter $d_{50} = 1.14$ mm with $\sigma_g = 1.45$, and a median diameter $d_{50} = 2.18$ mm with $\sigma_g = 1.35$. The previous study (Guo et al. 2009) has shown that the scour depth in submerged flow is independent of the number of girders so that only a six-girder deck was tested in this study. The deck had rails at the edges that could pass overflow on the deck surface whose elevation was adjustable, permitting the deck to have eight different inundation levels. A LabView program was used to control an automated flume carriage that was equipped with an Micro Acoustic Doppler Velocimeter (MicroADV) for records of velocities and a laser distance sensor for records of depths of flow and scour. The MicroADV (SonTek 1997) measures 3-dimensional flow in a cylindrical sampling volume of 4.5 mm in diameter and 5.6 mm in height with a small sampling volume located about 5 cm from the probe; the range of velocity measurements is from about 1 mm/s to 2.5 m/s. In this experiment, velocity measurements were taken in a horizontal plane located at a cross-section 22 cm upstream of the bridge. The LabView program was set to read the MicroADV probe and the laser distance sensor for 60 seconds at a scan rate of 25 Hz. According to the users manual, the MicroADV has an accuracy of $\pm 1\%$ of measured velocity, and the laser distance sensor has an accuracy of ± 0.2 mm.

Two discharges were applied in the experiments. They were determined

Table 1: Experimental conditions

Approach flow conditions:	$h_u = 25\,\mathrm{cm}$, $R_h = 13.9\,\mathrm{cm}$
	$V_u = 42.5\,\mathrm{cm/s}$, $d_{50} = 1.14\,\mathrm{mm}$, $\sigma_g = 1.45$, $\mathrm{Re} = 59100$, $\mathrm{Fr} = 0.271$
	$V_u = 48.2\,\mathrm{cm/s}$, $d_{50} = 2.18\,\mathrm{mm}$, $\sigma_g = 1.35$ $\mathrm{Re} = 66700$, $\mathrm{Fr} = 0.308$
Bridge opening heights:	$h_b = 13, 16$, and 19 cm
Scour measurements at:	$t = 0.5, 1, 2, 4, 8, 12, 16, 20, 24, 30, 36$, and 42 hours

Note: Re is based on hydraulic radius, and Fr based on flow depth.

by a critical velocity and the flow cross-section in the test channel. The critical velocity was preliminarily calculated by Neill's (1973) equation and adjusted by a trial and error method. The critical velocity of sediment $d_{50} = 1.14$ mm was approximately 0.425 m/s and the corresponding experimental discharge Q was 0.0669 $\mathrm{m^3/s}$. The critical velocity of sediment $d_{50} = 2.18$ mm was approximately 0.482 m/s and the corresponding experimental discharge was 0.0759 $\mathrm{m^3/s}$. To study the scour processes, scour morphologies at eleven times were measured for each given bridge opening height. The settings of the flow, sediment, bridge height and designated times are listed in Table 1, where the Froude and Reynolds numbers mean the approach flows were subcritical turbulent flows.

For each test with designated bright height and scour time, it was proceeded as follows: 1) Filled the sediment recess with sand and evenly distributed sand on the bottom of the flume until the depth of sand was 60 cm in the sediment recess and 20 cm in the test channel. 2) Installed a bridge deck at a designated elevation and positioned it perpendicular to the direction of flow. 3) Pumped water gradually from the sump to the flume to the experimental discharge that was controlled by the LabView. 4) Checked the approach velocity distributions in the vertical and lateral to see if they were more or less uniform away from the walls, and ran each test until the designated time. 5) Gradually emptied water and carefully removed the model bridge from the flume. 6) Scanned the 3-dimensional scour morphology using the laser distance sensor with a grid size of $5\,\mathrm{cm} \times 5\,\mathrm{cm}$.

Results and Discussion

The major results were the time-dependent variations of 3-dimensional scour morphology, which were documented in a huge MS Excel file and will be published in the web site of the FHWA Hydraulics Lab. A representation of 3-dimensional scour processes at different times is shown in Figure 1, and the corresponding width-averaged longitudinal scour profiles are shown in Figure 2. Both figures show that: (1) The shape of the scour holes remains almost unchanged as time elapses. (2) The scour hole develops rapidly from $t = 0$ to 0.5 hrs, which means the rate of change of scour depth is very large at the beginning of scour. (3) The scour depth increases as time elapses, but at $t = 30 - 42$ hrs the change of scour depth is negligible and the rate of change tends to zero, which implies that an

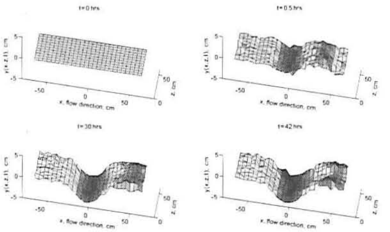

Figure 1. Scour evolution

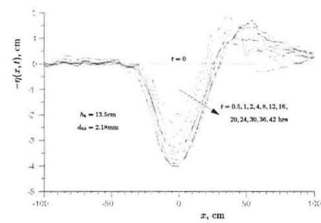

Figure 2. Width average scour profiles

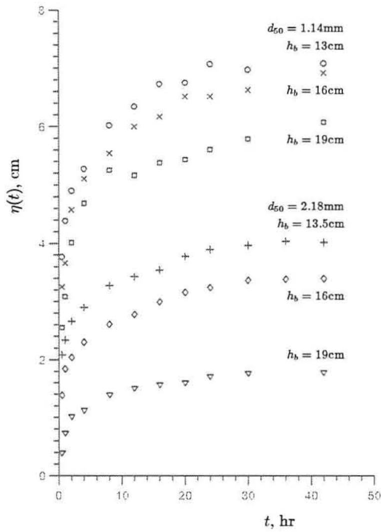

Figure 3. Maximum scour depth

equilibrium scour hole was attained approximately at $t = 30 - 42$ hrs. (4) The position of the maximum scour depth is close to the outlet of the bridge, at $x = -0.5$ to 0 cm, where $x = 0$ is 4 cm from the downstream face of the bridge. (5) In general, the scour morphology is approximately 2-dimensional before the maximum scour depth but 3-dimensional after the maximum scour depth.

For engineering concerns, the most important is the time-dependent variation of the maximum scour depths, which are summarized in Figure 3 that again shows as time elapses, the maximum scour depth, $\eta(t)$, increases but the rate of change decreases and tends to zero as an equilibrium scour approaches. Further discussion of the maximum scour depths is addressed in next section.

SEMI-EMPIRICAL MODEL FOR MAXIMUM SCOUR DEPTH

Scour processes are described by the conservation of mass for sediment, which is often called the Exner equation (Paola and Voller 2005). For one-dimensional flow, it is written as

$$-c_b \frac{\partial \eta}{\partial t} + \frac{\partial q_s}{\partial x} = 0 \tag{1}$$

where c_b = bedload concentration, η = scour depth at time t (Figure 4), q_s = volumetric sediment transport rate per unit width, and x = coordinate in the flow direction. Assume that scour processes in clear water are mainly due to bedload transport, the sediment transport rate, q_s, in Eq. (1) can then be approximated

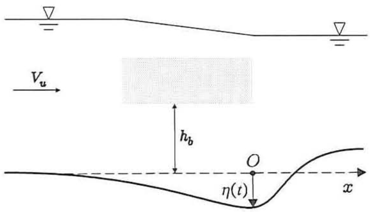

Figure 4. Definition of scour depth

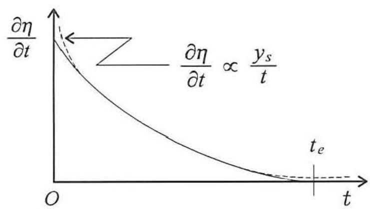

Figure 5. Sketch of scour rate

by the Meyer-Peter equation (Chien and Wan 1999, p339)

$$\frac{q_s}{\sqrt{(s-1)\,gd_{50}^3}} = 8\left(\frac{\tau_0 - \tau_c}{(s-1)\,\rho g d_{50}}\right)^{3/2} \tag{2}$$

where s = specific gravity of sediment, g = gravitational acceleration, d_{50} = diameter of sediment, $\tau_0 = \tau_0\,(x,t)$ = bed shear stress varying with location x and time t, τ_c = critical shear stress for bedload motion, and ρ = density of water.

Substituting Eq. (2) into Eq. (1) and rearranging it gives

$$\frac{\partial \eta}{\partial t} = \frac{12}{(s-1)\,c_b}\sqrt{\frac{\tau_0 - \tau_c}{\rho}}\left(\frac{1}{\rho g}\frac{\partial \tau_0}{\partial x}\right) \tag{3}$$

where

$$\tau_0 = \frac{f}{8}\rho V_b^2 \tag{4}$$

in which f = friction factor that varies with a Reynolds number and relative roughness, and V_b = cross-sectional average velocity under a bridge, which varies spatially and temporally. Eqs. (3) and (4) show that the rate of change of scour depth depends on the flow condition, $V_b\,(x,t)$, and sediment (packing density c_b, critical shear stress τ_c, and friction factor f). At the beginning, $t=0$, of a scour process, the value of $\partial\eta/\partial t$ is large and positive since $\tau_0 > \tau_c$ and $\partial\tau_0/\partial x > 0$ (because downstream transport rate is always larger during a scour phase); after that, the value of $\partial\eta/\partial t$ decreases with time since both $\tau_0 - \tau_c$ and $\partial\tau_0/\partial x$ decrease with time; finally, the value of $\partial\eta/\partial t$ becomes zero when an equilibrium scour depth is attained. Accordingly, the rate of change of scour depth, $\partial\eta/\partial t$, can be represented by the solid line in Figure 5 where t_e = equilibrium time.

Theoretically, the solution of Eq. (3) must be coupled with a flow equation that describes the spatial and temporal variation of velocity $V_b\,(x,t)$ under a bridge. Nevertheless, the nonlinear interaction between scour depth and velocity under a bridge makes an exact solution for η impossible. For engineering concern, this analysis focuses on the temporal variation at the maximum scour depth where $x=0$, i.e., $\eta = \eta(0,t)$. According to Figure 5, as a first approximation in the middle of a scour phase, one can hypothesize

$$\frac{\partial \eta}{\partial t} \propto \frac{y_s}{t} \tag{5}$$

where the equilibrium scour depth y_s, which is related to flow conditions and has been discussed in Guo et al. (2009), is introduced since it is an appropriate scaling length of scour depth η. Eq. (5) is represented by the dashed line in Figure but it is not valid at $t = 0$ and $t = t_e$. Eq. (5) may be rewritten as

$$\frac{\partial \eta}{\partial t} = \frac{k y_s}{t} \tag{6}$$

where the constant k reflects the effect of sediment, as suggested by c_b, τ_c and f in Eqs. (3) and (4).

Integrating Eq. (6) and rearranging it gives

$$\frac{\eta}{y_s} = k \ln t + B \tag{7}$$

where the integration constant B is approximately determined by the equilibrium condition, $\eta = y_s$ at $t = t_e$. Substituting this condition into Eq. (7) results in

$$B = 1 - k \ln t_e \tag{8}$$

Eq. (7) then becomes

$$\frac{\eta}{y_s} = k \ln \frac{t}{t_e} + 1 \tag{9}$$

which means in the middle of a scour process, the evolution of scour depth approximately follows a log law, like the law of wall in turbulent boundary layers.

Note that although the constant B in Eq. (8) is determined at $t = t_e$, Eq. (9) should not be valid at $t = 0$ and $t = t_e$ due to the hypothesis of Eq. (5), as shown in Figure 5. Fortunately, the scour depth at $t = 0$ is insignificant in practice so that one can leave this flaw alone. The second flaw at $t = t_e$ can be fixed by analogizing it to the modified log-wake law in turbulent boundary layers (Guo and Julien 2003, Guo et al. 2005), which means one can force the rate of change of scour depth to be zero at $t = t_e$ by adding a cubic function to Eq. (9)

$$\frac{\eta}{y_s} = k \left[\ln \frac{t}{t_e} - \frac{1}{3} \left(\frac{t}{t_e} \right)^3 + \frac{1}{3} \right] + 1 \tag{10}$$

where the equilibrium time t_e is characterized by the overall flow conditions and may be expressed by

$$t_e = C \frac{h_b}{V_u} \tag{11}$$

where C is an undetermined constant, h_b = bridge opening height before scour (Figure), and V_u = approach velocity. Substituting Eq. (11) into Eq. (10) gives

$$\frac{\eta}{y_s} = k \left[\ln \frac{t V_u}{C h_b} - \frac{1}{3} \left(\frac{t V_u}{C h_b} \right)^3 + \frac{1}{3} \right] + 1 \tag{12}$$

which is called the log-cubic law for time-dependent scour depth.

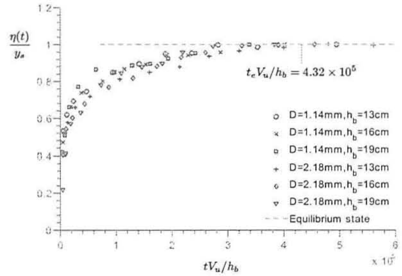

Figure 6. Test of similarity hypothesis

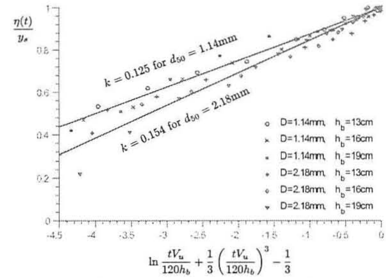

Figure 7. Determination of k values

One can summarize the above with the following hypothesis: Time-dependent scour depth may be described by a log-cubic law, Eq. (12), where the scour depth η is scaled by its equilibrium depth y_s, the time t is scaled by the approach velocity V_u and bridge opening height h_b, and the parameter k may increase with increasing sediment size while the parameter C may be a universal constant.

TEST OF SEMI-EMPIRICAL MODEL

To test the hypothesis, the present experimental data are, first, plotted according to η/y_s versus tV_u/h_b in Figure 6, which demonstrates that the scour depth η and time t are indeed appropriately scaled by y_s and h_b/V_u, respectively. The equilibrium state is, next, read from Figure 6 where

$$\frac{t_e V_u}{h_b} \approx 4.32 \times 10^5 \tag{13}$$

which gives the constant C in Eq. (11) as

$$C \approx 4.32 \times 10^5 \tag{14}$$

One can, then, clearly see from Figure 6 that most of the data points for $d_{50} = 1.14\,\text{mm}$ (blue) are above those for $d_{50} = 2.18\,\text{mm}$ (red), which just confirms the hypothesis that the value of k increases with increasing sediment size (since the value of the brackets of Eq. (12) is negative). Furthermore, using a nonlinear least-squares method in MatLab, fitting Eq. (12) to the present data gives

$$\begin{aligned} k &= 0.125 \quad \text{for } d_{50} = 1.14\,\text{mm} \\ k &= 0.154 \quad \text{for } d_{50} = 2.18\,\text{mm} \end{aligned} \tag{15}$$

which are shown in Figure 7 through the slopes. Finally, the model parameters in Eqs. (14) and (15) can well fit the log-cubic law, Eq. (12), to the data in Figures 8 and 9 for $d_{50} = 1.14\,\text{mm}$ and $2.18\,\text{mm}$, respectively. The corresponding correlation coefficients, R^2, and standard deviations, σ, are as follows:

$$\begin{aligned} R^2 &= 0.982, \quad \sigma = 0.030, \quad \text{for } d_{50} = 1.14\,\text{mm} \\ R^2 &= 0.963, \quad \sigma = 0.036, \quad \text{for } d_{50} = 2.18\,\text{mm} \end{aligned}$$

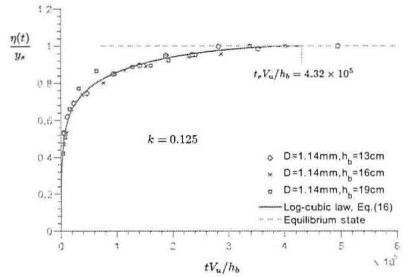

Figure 8. Test of Eq. (12) with $d_{50} = 1.14\,\text{mm}$

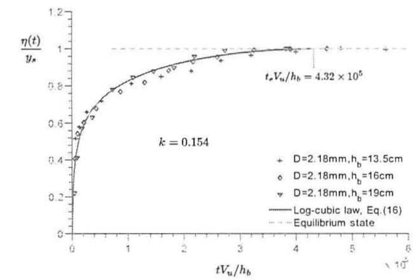

Figure 9. Test of Eq. (12) with $d_{50} = 2.18\,\text{mm}$

which implies that with a 68% confidence interval, the estimated scour depth has an error of $\pm\,(3-4)\,\%$ of equilibrium depth y_s; and with a 95% confidence interval, the estimated scour depth has an error of $\pm\,(6-7)\,\%$ of equilibrium depth y_s.

One can conclude that the log-cubic law, Eq. (12), indeed describes the time-dependent scour depth under bridge-submerged flow where the parameter C is a universal constant, but the parameter k increases with increasing sediment size. Because of the limitation of sediment sizes, a general relationship between the parameter k and sediment size d_{50} cannot be generated in this study.

IMPLICATION AND LIMITATION

Current practice for determining the scour depth at a bridge crossing is based on the equilibrium scour depth of a design flood (e.g., 50-year, 100-year, and 500-year flood events), which is unnecessarily larger than a real maximum scour depth during a bridge life span since the peak flow period of a flood event is often much shorter than its equilibrium time. The proposed method can be used to estimate the evolution of scour depth at a certain time, which means it can appropriately reduce the design depth and construction cost of a bridge foundation according to design flow and a peak flow period. Nevertheless, the proposed method is limited to steady flow with clear water conditions and uniform bed materials. Its applications to unsteady flow (hygrograph) and live-bed conditions is the next step of this research in the future.

Besides, when applying Eq. (12) to practice, one has to note that: (1) the equilibrium scour depth y_s is estimated by Guo et al. (2009) although the measured values were used in the present study; and (2) the proposed method is only valid for

$$\frac{tV_u}{h_b} \leq 4.32 \times 10^5 \tag{16}$$

when $tV_u/h_b > 4.32 \times 10^5$, the equilibrium scour depth is used where $\eta = y_s$.

CONCLUSIONS

The following conclusions can be drawn from this study: (1) The shape of the longitudinal scour profiles remains almost unchanged with respected to time, shown in Figures 1 and 2. (2) The position of the maximum scour depth quickly moves to its equilibrium position that is close to the downstream edge of the bridge deck. (3) The rate of change of scour depth decreases as time elapses and tends to be zero as the scour approaches to its equilibrium state, as shown in Figure 3 by the change of slope. (4) The maximum scour depth can be described by two similarity numbers where the time-dependent scour depth is scaled by the corresponding equilibrium scour depth, and the time by the approach velocity and bridge opening height, as shown in Figure 6. (5) The time-dependent scour depth can be estimated by the log-cubic law, Eq. (12), which agrees very well with the collected flume data (Figures 8 and 9). (6) The proposed method may be used to estimate the evolution of scour depth at a certain time, which can appropriately reduce the design depth and construction cost of a bridge foundation according to design flow and a peak flow period.

ACKNOWLEDGMENTS

This study was financially supported by the FHWA Hydraulics R&D Program with Contract No. DTFH61-04-C-00037. The writers would like to thank Mr. Oscar Berrios for running a part of the tests and collecting the scour data for sediment $d_{50} = 2.18\,\mathrm{mm}$.

REFERENCES

Arneson, L. A., and Abt, S. R. (1998). "Vertical contraction scour at bridges with water flowing under pressure conditions." *Transportation Research Record.* 1647, 10-17.

Chang, W. Y., Lai, J. S., and Yen, C. L. (2004). "Evolution of scour depth at circular bridge piers." *J. Hydraul. Res.*, 130(9), 905-913.

Chien, N., and Wan, Z. (1999). *Mechanics of Sediment Transport.* ASCE Press.

Coleman, S. E., Lauchlan, C. S., and Melville, B. W. (2003). "Clear-water scour development at bridge abutments." *J. Hydraul. Res.*, 41(5), 521-531.

Dargahi, B. (1990). "Controlling mechanism of local scouring." *J. Hydraul. Engrg.*, 116(10), 1197-1214.

Dey, S., and Barbhuiya, A. K. (2005). "Time variation of scour at abutments." *J. Hydraul. Engrg.*, 131(1), 11-23.

Guo, J., and Julien, P. Y. (2003). "Modified log-wake law for turbulent flow in smooth pipes." *J. Hydraul. Res.*, 41(5), 493-501.

Guo, J., Julien, P. Y., and Meroney, R. N. (2005). "Modified log-wake law for zero-pressure-gradient turbulent boundary layer." *J. Hydraul. Res.*, 43(4), 421-430.

Guo, J., Kerenyi, K., Pagan-Ortiz, J., and Flora, K. (2009). "Submerged-flow bridge scour under maximum clear-water conditions." Submitted to *J. Hydraul. Engrg.*

Kothyari, U. C., Garde, R. C., and Raju, K. G. R. (1992). "Temporal variation of scour around circular bridge piers." *J. Hydraul. Engrg.*, 118(8), 1091-1106.

Lai, J. S., Chang, W. Y., Yen, Y. L. (2009). "Maximum local scour depth at bridge piers under unsteady flow." *J. Hydraul. Engrg.*, 135(7), 609-614.

Lopez, G., Teixeira, L., Ortega-Sanchez, M., and Simarro, G. (2006). "Discussion: Further results to time-dependent local scour at bridge elements." *J. Hydraul. Engrg.*, 132(9), 995-996.

Lyn, D. A. (2008). "Pressure-flow scour: a re-examination of the HEC-18 equation." *J. Hydraul. Engrg.*, 134(7), 1015-1020.

Melville, B. W. (1992). "Discussion: Study of time-dependent local scour around bridge piers." *J. Hydraul. Engrg.*, 118(11), 1593-1595.

Melville, B. W., and Chiew, Y. M. (1999). "Time scale for local scour at bridge piers." *J. Hydraul. Engrg.*, 125(1), 59-65.

Oliveto, G., and Hager, W. H. (2002). "Temporal evolution of clear water pier and abutment scour." *J. Hydraul. Engrg.*, 128(9), 811-820.

Oliveto, G., and Hager, W. H. (2005. "Further results to time-dependent local scour at bridge elements." *J. Hydraul. Engrg.*, 131(2), 97-105.

Paola, C., and Voller, V. R. (2005). "A generalized Exner equation for sediment mass balance." *J. Geophys. Res.*, 110, F04014.1-F04014.8.

SonTek. (1997). *Acoustic Doppler velocimeter technical documentation, version 4.0*, SonTek, San Diego.

Yanmaz, A. M. (2006). "Temporal variation of clear water scour at cylindrical bridge piers." *Can. J. Civ. Eng.*, 33, 1098-1102.

Yanmaz, A. M., and Altmbilek, H. D. (1991). "Study of time-dependent local scour around bridge piers." *J. Hydraul. Engrg.*, 117(10), 1247-1268.

Yanmaz, A. M., and Kose, O. (2009). "A semi-empirical model for clear-water scour evolution at bridge abutments." *J. Hydraul. Res.*, 47(1), 110-118.

In *Situ* Measurement of the Scour Potential of Non-Cohesive Sediments (ISEP)

Cary Caruso[1] and Mohammed Gabr[2], FASCE

[1]Graduate Student, Department of Civil, Construction and Environmental Engineering, North Carolina State University, Box 7908, Mann Hall, Stinson Drive, Raleigh, NC 27695-7908 ; PH (919)479-3236; e-mail: cwcaruso@unity.ncsu.edu
[2]Alumni Distinguished Professor, Department of Civil, Construction and Environmental Engineering, North Carolina State University, Box 7908, Raleigh, NC 27695-7908; PH. (919)515-7904; e-mail:gabr@eos.ncsu.edu

ABSTRACT

A vertical probe (VP) employing a water jet has been developed for assessing scour potential and scour rates of sediments typically found at the bottom of rivers or streams. The probe termed "In situ Scour Evaluation Probe," or ISEP, is based on the idea that analysis of the probe penetration rate into the soil may be correlated with scour rate and erosion potential. The method proposed herein aims at measuring the potential scour rate *in situ* and as a function of depth. Results on the test sand with mean particle diameter (D_{50}) ~0.3 mm suggest that the rate of advancement of the probe can be empirically correlated to the vertical velocity of the water at the tip of the probe raised to a positive exponent. For the saturated sand used in testing, the exponent appears to be 1.4. The rate of probe advancement seems to also vary with moisture content. Thus far, scour rates determined with this proposed method are found to be in reasonable agreement with scour rates published for similar sand type.

INTRODUCTION

Scour evaluation is critical for assessing the stability of several types of civil infrastructures prior to, and after, storm events, as was learned from failures during and after Hurricane Katrina (Seed et al, 2006). Briaud (2002) suggests that 60% of all the bridge failures in the US are caused by excess scour under the bridge piers or abutments leading to collapse or serious structural damage. Figure 1 shows an example of a bridge failure near Toyah, TX due to scouring of the foundation soil due to flooding during a thunderstorm (NWS, 2004).

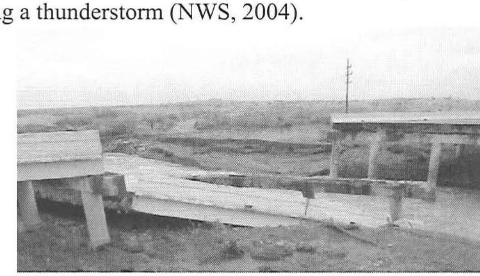

Figure 1. Collapse of the I-20 Bridge Near Toyah, Texas on 4/4/2004. (Downloaded from: NWS Midland/Odessa (2004)

Moreover, assessment of scour potential is a persistent challenge for the engineering profession across disciplines. For example, scour cases were cited for civil engineering by Seed et al (2006), agricultural engineering by Hanson and Hunt (2007) and petroleum engineering by Vardoulakis, et al (1996).

Current techniques for measuring scour potential require either removal of soil samples for laboratory testing such as the Erosion Function Apparatus (EFA) proposed by Briaud et al (2001), or limiting measurements to scour on the surface of the sediment using inverted flumes, e.g. Aberle et al. (2003), or the use of surface jets as was presented by Hanson et al (2002) and Hanson and Cook (2004).

PROPOSED SCOUR PROBE

The process proposed here for the development of ISEP uses the method of a vertical water jet driven by a pump to erode the soil and advance the probe into the profile. Cone-tipped stainless steel pipe sections are attached to a digitally controlled, centrifugal pump providing controllable and repeatable vertical water velocity at the tip. As the vertical water jet is deflected by the soil, the now horizontally moving water applies a shear stress to the soil grains causing erosion. A schematic of the probe and a photograph of the tips are shown in Figure 2a and 2b.

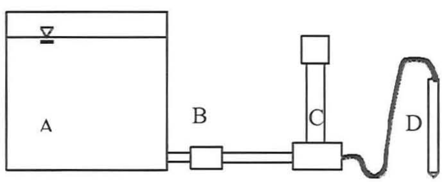

Figure 2a. Schematic of the vertical scour apparatus: A. Reservoir B. Ball Valve C. Pump D. Probe and tip

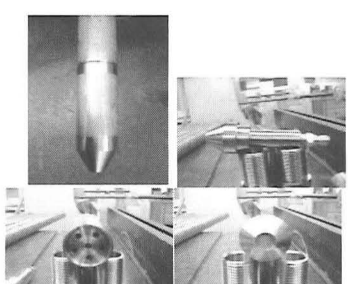

Figure 2b. Tips used in the collection of data for the current research.

Generally, the design goal is the development of a portable system allowing the assessment of soil scourbility profile at key locations near critical infrastructures. Accordingly, both an assessment of current conditions as well as tracking of erodibility changes with various velocity-time profiles are to be achieved. The proposed scour probe and ancillary equipment use off-the-shelf parts except for the probe body and tips, which were constructed in the NCSU precision machine shop. The probe has a stainless steel body with several removable stainless steel tips. The probe body was designed in 1.22 m (4 ft) sections so that it may be broken down for transport and can conveniently handled in the field. The pump is Gould GLSSV2 variable speed centrifugal pump coupled to an ITT PumpSmart variable speed pump controller.

Several tips and configurations were constructed and tested. The flat-topped tip with 6 - 0.00635 m (1/4 in) orifices was found to give the best penetration in dry sand. However, for the saturated sand used in the majority of testing, the 60° truncated cone tip with a 0.0127 m orifice (1/2 in) gave the most consistent results. A 0.003175 m (1/8 in) tip was constructed and found to be restrictive to water flow so further testing was suspended. Another tip with a 0.01905 m (3/4 in) orifice in a truncated cone configuration has been constructed to allow for the application of lower water velocities with relatively high flow rates.

BACKGROUND - SOIL SCOUR

The scour of granular materials has been discussed extensively in the literature. Albert Shields (1936) described the initiation of motion of granular particles on the basis of flume testing during his PhD research, as presented in Kennedy (1991). One of Shields' conclusions was that a critical shear stress (τ_c) existed below which particles will not be dislodged and moved. This critical shear stress value represents the viscous drag imparted by the moving fluid to the bed particles, and is related to a critical velocity. The critical velocity necessary to create a given shear stress is a function of the depth of flow and the particle diameter, and according to Richardson and Davis (2001) is given as:

$$V_c\ (m/s^2) = 6.19 y^{1/6} d_{50}^{\ 1/3} \quad (1)$$

where: d_{50} = size of the bed material, and y is the depth of flow. Another factor controlling the erosion of granular soils is the resisting force of a particles submerged weight (the submerged weight is the difference between the gravitational weight of the particle and the buoyancy force on the particle.) For such particles, erosion or scour will occur when the drag force exceeds the force of friction of stacked particles. Briaud (2001) discussed the observation in slow-motion video of erosion experiments in flumes in which the dominant means of particle motion are sliding, rolling, and plucking; Shields' basic equation stated that the critical shear stress (τ_c) is related to particle diameter and was given by:

$$\tau_c\ (N/m^2) = 0.63 d_{50}\ (mm) \quad (2)$$

where: d_{50} = particle diameter corresponding to 50% is finer. This basic conclusion that the critical shear stress is proportional to d_{50} has been mostly supported by others including White (1940), Laursen (1962) and Wiberg and Smith (1987); only the proportionality constant differs. Briaud et al (1999) suggested that the proportionality constant is one with the following equation for τ_c:

$$\tau_c\ (N/m^2) = d_{50}\ (mm) \tag{3}$$

where d_{50} = particle diameter where 50% is finer is more appropriate for sands. For gravels, with diameters ranging between d_{50} = 4.89 − 31.75 mm, Dey and Raju (2002) suggested a non-dimensional shear stress of:

$$t = \tau_b/(\Delta g \rho d_e) = 0.013\ F_d^{\ 2} d^{0.48} h^{0.49} \tag{4}$$

where: F_d is the particle Froude number, d is the effective particle diameter, and h is the water depth to the top of the virtual bed, τ_b = bed shear stress, g = gravitational constant, ρ = particle density and Δ = s-1, s = relative density of the particles. Regardless of the particular form, particle size is one of the controlling factors in describing a soil's ability to resist scour or erosion since it plays an important role in both a particle's weight and the effective surface area exposed to the moving fluid.

Cohesive sediments are somewhat more complicated since additional forces are involved. These attractive-repulsive forces are mostly electrical in nature and include electrostatic and van der Waal's forces. Briaud (1999b) showed that ratio of van der Waal's forces to gravitational forces is 10^{-20} for sands but only 10^{-3} for clays.

Stein et al (1993) derived an expression for the shear stress applied to a surface within the potential core of the jet as:

$$t_e = C_f r\, U_0^{\ 2} \tag{5}$$

where: t_e = applied shear stress to bed, C_f is the friction coefficient determined by Robinson (1992) and is equal to $(0.0474/2)R_0^{\ -1/5}$, $R_0 = 2y_0U_0/n$, U_0 = Vertical velocity of water at the tip, r = density, y_0 = jet thickness. This equation was also derived by Aderibigbe & Rajaratnam (1997) and is used in this paper as the basis for conversion between vertical water velocity and bed shear stress.

BACKGROUND-JET SCOUR AND VERTICAL WATER JET

The use of vertical water jets to measure erosion is not a new concept. The earliest published use the authors found is by Dunn (1959), which was a laboratory study of the cohesive strength of stream sediments. Moore and Masch (1962) also developed a laboratory device for measuring scour using vertical water jets. Patterson (1989) described a "Cohesive Strength Meter" using pulsating water jets for measuring the in situ erosion shear stress of intertidal sediments. More recently, Hanson et al (2002) and Hanson and Cook (2004) have described an apparatus also using a vertical jet for measurement of scour. This device and the resulting stress distribution are shown in Figure 3. It has long been recognized that scour downstream of many hydraulic structures such as culverts and spillways maybe analogues to jet scour. Consequently, this has been a topic of research over many years. Doodiah et al (1953), Sarma (1965), Beltaos, and Rajaratnam (1974), Aderibigbe & Rajaratnam (1997) and many others have all made contributions to this field. Most of these studies were concerned with the problem of describing the maximum scour depth as the jet is held stationary. For these cases, the height of the jet above the surface is greater than the length of the "potential core" as defined by Albertson et al (1948).

The "potential core" is that part of the jet where water retains its original velocity. At distances greater than the potential core, the velocity of flow decreases linearly as was presented by Albertson et al (1948). Niven and Khalili (1998) took a different approach and investigated internal jets or jets submerged within the material. While their analysis was concerned with in situ fluidization of sand beds, one of their conclusions was that the penetration depth for an embedded jet was related to scour beneath the jet, and may be described by a Shields-type of scour.

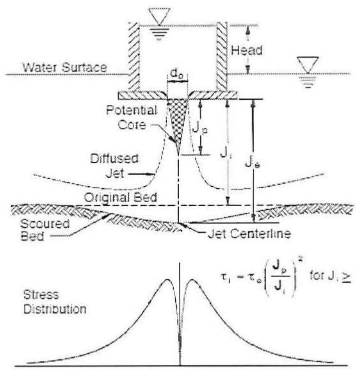

Figure 3. Schematic of vertical jet apparatus and the resulting stress distribution, from Hanson and Cook (2004).

TESTING AND RESULTS

The sand used in testing is characterized by the grain size distribution shown in Figure 4. The D_{50} value for this sand is about 0.3 mm. The angle of internal friction for this sand was also determined in the lab and was found to be about 37°. Critical shear stress can be calculated assuming a 'depth' equal to the diameter of the probe. Applying Equation (1) to the sand parameters suggests a critical velocity of 0.25 m/s. If the analysis from Stein et al (1993) (summarized in Equation 5) is applied to this velocity, the resulting critical shear stress is about 0.3 N/m^2. If Shields relationship, Equation (2), is used, the calculated critical shear stress is 0.189 N/m^2. Using Briaud's (1999) relationship (equation 3) yields a critical shear stress of 0.3 N/m^2.

Results from calibration tests collected with the curent ISEP configuration are shown in Figure 5 along with several of the regression equations derived from this data set. The pump is controlled by setting the RPM, and the water velocities from the tip are used to calculate the shear stresses applied to the soil. The water velocities obtained with the current tips range between 2.4 and 5.8 m/s and all subsequent results were collected with these tips in this velocity range.

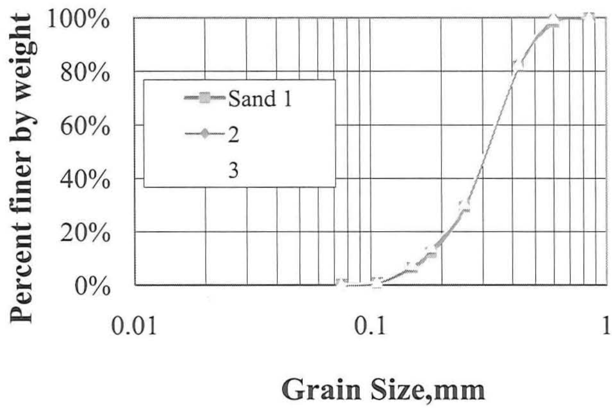

Figure 4 Grain size distribution of the sand used in testing.

A new tip with a larger orifice (0.01905 m or 3/4 inch) has been constructed and is currently being tested. The expected water velocities from this tip are shown on the calibration chart in Figure 5 as the lowermost (blue) line. The use of the new tip should reduce the water velocities into the 1.0 to 2.5 m/s range.

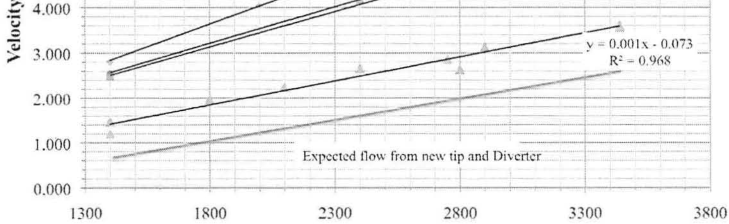

Figure 5. Calibration results relating pump RPM to water velocity. The blue line shows the expected velocities with the new, larger tip currently under

The penetration rate vs shear stress measured with the ISEP is shown in Figure 6. The data shown are determined by measuring the time taken for 5 cm of embedment of the probe as it progresses into the soil. Two trends are apparent in spite of the scatter. First, as the shear stress increases, the erosion rate, indicated by the penetration rate, increases. Secondly, as the probe progresses deeper into the soil, the rate at which the probe embeds itself decreases.

In Figure 7, the penetration rate versus water velocity is shown overlain with Briaud's (2008) proposed erosion categories. Also shown on the graph are results from Erosion Function Apparatus (EFA) measurements of sand with a similar D_{50} ~0.3 mm (Briaud et al (2004). While it is tempting to suggest that the data are sub-parallel with the EFA data, this conclusion would be premature. However,

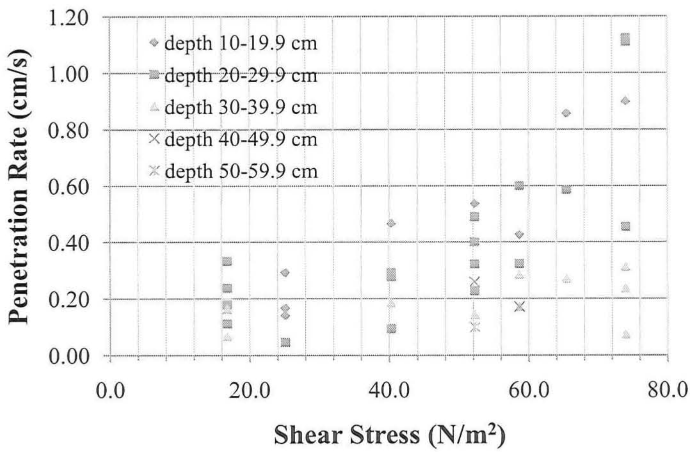

Figure 6. Penetration rate vs. Shear Stress displayed as a function of

examination of published EFA results show that a gradual decrease in slope as water velocity increases is not uncommon. Examples of this behavior were also observed in results published by Briaud (2008), Seed et al (2006) and others. The use of the new tip mentioned previously should decrease tip water velocities allowing data to be collected with velocities down to 1.0 m/s allowing results to be directly compared.

Figure 8 shows the results of transforming the scour rate data (shown in Figure 7) using the Stein and Nett equation (Equation 5), such that the independent variable is now shear stress. In Figure 8, the same general behavior is observed as in Figure 7. An additional, non-quantitative observation was made early during testing of the vertical scour probe. When higher flow rates were used (> 5.8 m/s~17 L/min), the saturated sand would liquefy and the probe would embed its entire length into the soil. This behavior became less likely as the water velocity was decreased.

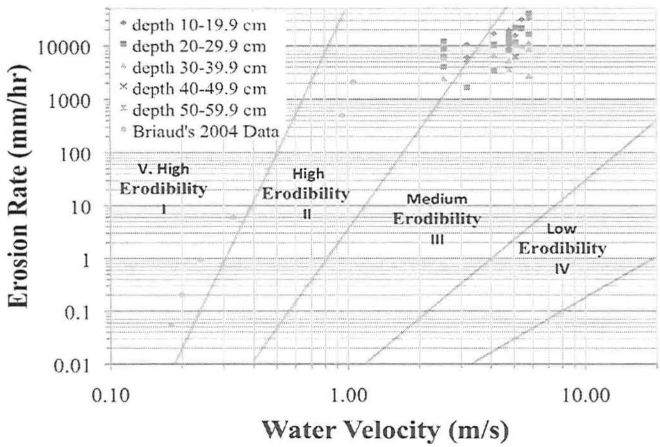

Figure 7 Erosion rate versus water velocity for the data collected here (data are also shown for a similar sand referenced in Briaud et al, 2004).

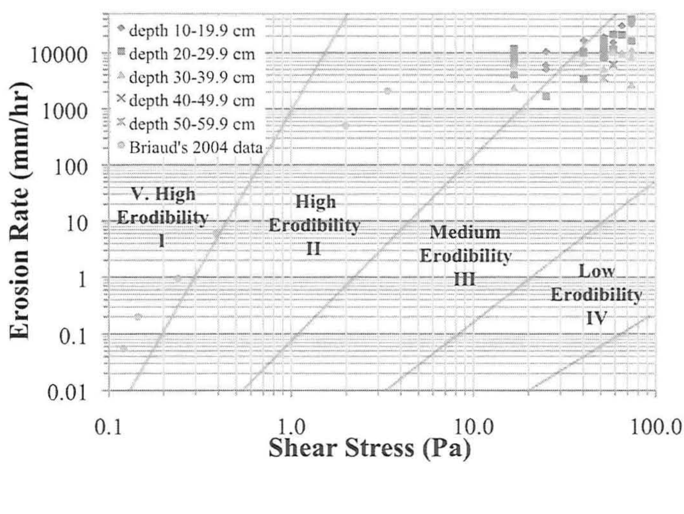

Figure 8 Erosion rate versus shear stress (For comparison, data for a similar sand referenced in Briaud et al (2004) and Briaud's (2008) are also shown.

SUMMARY AND CONCLUSIONS

A vertical probe employing a water jet has been developed for measuring scour potential and erosion rates of non-cohesive sediments, the probe termed "In situ Scour Evaluation Probe," or ISEP is proposed for in situ assessment of scour potential with depth. The probe has been tested in sand across a wide range of water velocities at the tip. These water velocities have been used to estimate a range of shear stresses applied to the surface below the tip, and the scour rates resulting from the water flow have been calculated. It is found that scour rates determined on the test sand using the method described herein are similar to those measured and reported using the EFA method presented by Briaud (2001), although more testing is required for further assessment of the data obtained using the ISEP probe.

Work is in progress to apply this technique to deeper layers of soil and to assess the applicability of the technique to different soils. Different sands and different sand /fines mixtures will be tested to further assess and calibrate this technique. Various flow rates will also be applied to these soils since a different mechanism of scour is induced at different water velocities. In addition, the vertical probe will be deployed this summer to measure erosion rates along the beaches of the Outer Banks of North Carolina to attempt differentiation of those parts of the Outer Banks displaying different historical erosion rates during storms.

ACKNOWLEDGEMENT: This material is based upon work supported by the US Department of Homeland Security under Award Number: 2008-ST-061-ND 0001.

Disclaimer: The views and conclusions contained in this document are those of the authors and should not be interpreted as necessarily representing the official policies, either expressed or implied, of the US Department of Homeland Security.

REFERENCES

Aderibigbe, O.O. and Rajaratnam, N. (1997), 'Erosion of Loose Beds By Submerged Circular Impinging Vertical Turbulent Jets', *Journal of Hydraulic Research/De Recherches Hydrauliques*, 35 (4), 567-74.

Aberle, J, Nikora, V. McLean, S., Doscher, C., McEwan, I., Green, M., Goring, D., and Walsh, J., (2003), 'Straight Benthic Flow-Through Flume for In Situ Measurement of Cohesive Sediment Dynamics', *J. Hydr. Engr*. 129, (1) 63-67.

Beltaos, S and Rajaratnam, N. (1974), 'Circular Turbulent Impinging Jets.', J. Hyd. Div., Proc. ASCE, 100, HY 10, 1313-28.

Briaud, J.L., et al. (2001), 'Erosion Function Apparatus for Scour Rate Predictions', *Journal of Geotechnical and Geoenvironmental Engineering*, 127 (2), 105-13.

Briaud, J. L., (2002), TTI Researcher, V38, #4.

Briaud, J.L, Chen, H.C., Li, Y., Nurtjahyo, P. and Wang, J., (2004) Pier and Contraction Scour in Cohesive Soils, *NCHRP Report 516*, Transportation Research Board, Washington, D.C.

Briaud, J. L, (2008), 'The Ninth Annual Ralph B. Peck Lecture.' *Journal of Geotechnical and Geoenvironmental Engineering*, 134, (10), 1424-1447

Doddiah, D., Albertson, M. L., and Thomas, R. (1953). 'Scour from jets'. *Proc.,* *Minnesota Int. Hydrology Convention, International Association for Hydraulic Research*, Minneapolis, 161–169.

Dunn, I. S. 1959 'Tractive resistance of cohesive channels.' *ASCE. Journal of Soil Mechanics Found. Div.* Am. Soc. Civ. Eng. 85, 1–24.

Hanson, Gregory J., Robinson, K. M. and Cook, K. R. (2002),'Scour Below an Overfall: Part II.' Prediction', *Transactions of the American Society of Agricultural Engineers*, 45 (4), 957-64.

Hanson, G.J. and Cook, K.R. (2004), 'Apparatus, Test Procedures, and Analytical Methods to Measure Soil Erodibility in Situ', *Applied Engineering in Agriculture*, 20 (4), 455-62.

Hanson, G. J. and Hunt, S. L. (2007), 'Lessons Learned Using Laboratory Jet Method to Measure Soil Erodibility of Compacted Soils', *Applied Engineering in Agriculture*, 23 (3), 305-12.

Laursen, E. M. (1962). 'Scour at bridge crossings.' *Trans., ASCE*, Reston,Va., 127(3294), 166–209.

Moore, W. M. & Masch, D. M. 1962, 'Experiments on the scour resistance of cohesive materials'. *Journal of Geophysical Research*, 67, 1437–1499.

NWS Midland/Odessa (2004), Picture downloaded from http://www.srh.noaa.gov/maf/?n=events_040402-04_toyah

Niven, R.K. & Khalili, N. (1998), 'In situ fluidisation by a single internal vertical jet, *Journal of Hydraulic Research'*, 36(2), 199-228.

Paterson, D. M. 1989, 'Short term changes in the erodibility of intertidal cohesive sediments related to the migratory behaviour of epipelic diatoms.' *Limnology and Oceanography* 34, 223–234.

Plew, D., Debnath, K., Aberle, J., Nikora,V., Cooper, G., (2007), 'In Situ Flume for Studying Cohesive and Non-Cohesive Sediment Erosion', *Proceedings of the Congress-International Association for Hydraulic Research*, 32(1) (1), 70.

Rajaratnam, N. and Mazurek,K., (2003), 'Erosion of Sand by Circular Impinging Water Jets With Small Tailwater', *Jour. of Hydraulic Eng.*, 129 (3), 225-29.

Richardson, E. V., and Davis, S. R. (1995). 'Evaluating scour at bridges,'*Rep. No. FHWA-IP-90-017 (HEC 18)*, Fed. Highway Admin., Washington, D.C.

Robinson, K. M. 1992. 'Predicting stress and pressure at an overfall'. *Trans. ASAE* 35(2): 561–569.

Sarma, K.V.N. (1965), 'Simple Empirical Formula for Scour under Vertical Jets', *Irrigation and Power (India)*, 22 (1), 27-33

Seed, R. B. and 34 others, (2006), 'Investigation of the Performance of the New Orleans Flood Protection Systems in Hurricane Katrina on August 29, 2005', *Report to National Science Foundation under Grants No. CMS-0413327 and CMS-0611632.*

Stein, O.R., Alonso, C.V and Julien, P.Y. (1993), 'Mechanics of Jet Scour Downstream of a Headcut', *Journal of Hydraulic Research,* 31 (6), 723-38.

Vardoulakis, I., Stavropoulou, M. and Papanastasiou, P. (1996) 'Hydro-mechanical aspects of the sand production problem', *Transport in Porous Media,* 22, 225–244.

White, C. M. (1940). 'The equilibrium of grains on the bed of a stream', *Proc. Royal Soc. of London, London*, 174(958), 322–338.

Geotechnical Limit to Scour at Spill-through Abutments

R. Ettema[1], M. ASCE and T. Nakato[2], L.M. ASCE

[1]College of Engineering and Applied Science, the University of Wyoming, Laramie, WY 82071, PH: (307) 766-6458; e-mail: rettema@uwyo.edu
[2]Consulting Engineer, 618 Pine Ridge Road, Coralville, IA 52241; PH: (319) 351-2504; e-mail: mollusk007@gmail.com

ABSTRACT

For spill-through bridge abutments adjoining waterways, practically all field cases of failure attributable to scour show a geotechnical failure of the spill slope of earthfill embankment associated with the abutment. The extent of scour and the maximum scour depth attainable at an abutment indeed are limited by the geotechnical stability of the earthfill embankment at the abutment. For a given design flow, the stability of the embankment limits scour depth. The actual region of scour leading to embankment failure is itself unremarkable. Typically, scour depths at spill-through abutments are modest, at least when viewed after the flood event producing the scour, and when other factors such as channel morphology effects are excluded. Though numerous illustrations of scour at spill-through abutments show failed embankment and channel bank, methods currently available for estimating scour do not address the geotechnical aspects of scour at spill-through abutments. This paper presents a method for relating scour depth to the strength properties of an abutment's compacted earthfill embankment.

INTRODUCTION

This paper discusses important geotechnical aspects of spill-through abutment scour (Figure 1a), and shows that as scour deepens it reduces the stability of the abutment's earthfill spill-slope. When the slope is exceeded, spill-slope material slides into the scour region and the flow transports it away. Further deepening leads to more slope instability and erosion, until eventually, the erosion extends to the abutment column (Figure 1b). Still further erosion breaches the embankment, increasing the flow area, and relaxing flow velocities through the bridge waterway. In overall terms, scour at spill-through abutments can be characterized as being largely a geomechanics design concern, and less of a hydraulics concern. The paper outlines an approach to formulating the geotechnical limit to maximum scour depth at a spill-through abutment. The current investigation was conducted using a laboratory flume for three distinct scour conditions developed during the NCHRP 24-20 program (Ettema, et al. 2010).

LABORATORY INVESTIGATIONS

The laboratory experiments were conducted using a model channel fitted in a sediment re-circulating flume, 21.3-m long, 4.0-m wide, and 1.0-m deep. The flume accommodated the half width of a compound channel; i.e., the flume width = $0.5B$, where B is the entire width of the compound channel. The width of the floodplain was adjustable, and the floodplain surface could be erodible or fixed. The main channel had a bed of uniform medium sand. The variable erodible natures of floodplain and embankment at bridge sites were simulated by means of tests with the model channel configured in the following arrangements that bracket the variable erodibility of floodplain and embankment:

1. Fixed floodplain and the embankment, both taken to be practically resistant to erosion, whereas the main-channel bed was erodible;
2. Erodible floodplain and main channel bed (the two being formed of the same noncohesive sediment and equally erodible), with the embankment being erodible but armored with riprap stone; and,
3. Erodible floodplain and main-channel bed, with the embankment unarmored. The abutment was formed of the same noncohesive sediment as the main-channel bed.

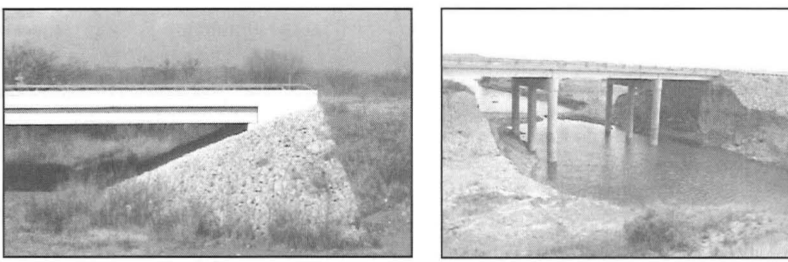

(a) (b)

Figure 1. A spill-through abutment with earthfill approach embankment on a floodplain (a); and observation of Scour Condition A for a spill-through abutment on floodplain, depicting bank and embankment failures (b).

The following prototype considerations and dimensions were used in selecting the model layout, length scale, and dimensions for both types of abutments:

- A road width of 12.0 m, in accordance with standard prototype two-lane roads. The road width includes 7.2 m plus 2.7 m-wide shoulders, a total width of 12.6 m;
- Pile spacing of 2 m to 3 m;
- Pile diameter of 0.3 m;
- The base of the pile cap submerged approximately 1.0 m below the original level of the floodplain bed;
- A 2-horizontal:1-vertical (2H:1V) constructed side slope of the earthfill embankment connected to the abutment; and,
- A 2H:1V slope of the bank between the floodplain and the main channel

Considerations of the flume's size led to selection of a geometrically undistorted length scale of 1:30 for the experiments. The model spill-through abutments were formed around a "standard-stub abutment," which consists of a concrete stub supported by a pile cap on two rows of circular pipes. The design and dimensions of standard-stub abutments commonly used by the Illinois, Iowa, and New York Departments of Transportation were used in the study.

SCOUR CONDITIONS CONSIDERED

Abutment scour may involve three distinct scour conditions (Ettema, et al. 2008; Ettema et al. 2010), herein termed Scour Conditions A, B, and C. These scour conditions were observed in the flume experiments and as well as at actual bridge sites:

- Scour Condition A occurs as scour of the main channel portion of a compound channel;
- Scour Condition B is scour of the floodplain, and occurs for abutments set well back from the main channel; and,
- Scour Condition C is a scour form that develops when breaching of an abutment's embankment fully exposes its abutment-column structure such that scour develops at the abutment column as if it were a pier.

For Scour Condition A, a useful analytical framework with which to relate maximum flow depth (incorporating maximum scour depth), Y_{MAX}, to flow conditions and boundary sediment or soil is to plot the dimensionless parameters Y_{MAX}/Y_C and q_2/q_1. Here, Y_C is the flow depth estimated for live-bed flow through a long contraction; q_2 is the area-average unit discharge of flow through the bridge section; and, q_1 is the area-average unit discharge of flow through the main channel upstream of the bridge site. At lower values of q_2/q_1, scour depth (and Y_{MAX}/Y_C) is governed by the local flow field around an abutment. However, for large values of q_2/q_1, scour development is governed by flow contraction, so that Y_{MAX}/Y_C asymptotically approaches about 1.1. The approximate 10 percent increase is attributable to local concentration of flow and turbulence generated by flow around the abutment.

For Scour Condition B, a useful analytical framework with which to relate maximum flow depth (incorporating maximum scour depth), Y_{MAX}, to flow conditions and boundary sediment or soil is to plot the dimensionless parameters Y_{MAX}/Y_C and q_{f2}/q_f. Here, Y_C is the flow depth estimated for clear-water flow through a long contraction; q_{f2} is the area-average unit discharge of flow through the floodplain portion of the bridge section; and, q_f is the area-average unit discharge of flow over the floodplain upstream of the bridge site. The trend for Y_{MAX}/Y_C versus q_{f2}/q_f is essentially the same for Y_{MAX}/Y_C and q_2/q_1.

For Scour Condition C, scour depths must be estimated in a semi-empirical manner similar to that used for estimating scour depth at a pier of complex geometry. Scour is governed by the highly three-dimensional flow field developed at an exposed pier-like column.

GEOTECHNICAL LIMIT TO MAXIMUM SCOUR DEPTH

The maximum scour depth attainable at an abutment is limited by the geotechnical stability of the earthfill embankment at the abutment. For a given design flow, scour cannot deepen below this limit. Figure 2 illustrates this limit in simple terms for an embankment set back on a floodplain. As scour deepens, it reduces the stability of the earthfill embankment at the abutment, adjusting the embankment slope to its equilibrium slope. When the slope is exceeded, embankment material slides into the scour region (Figure 2a) and the flow transports it away. Further deepening leads to more slope instability and erosion, until eventually, the erosion extends to the abutment column. Because the cross section of flow increases (Figure 2b), additional erosion results in breaching of the embankment and relaxation of the flow around the abutment.

It is possible to formulate the geotechnical limit to maximum scour depth. Figure 2 illustrates this limit. As indicated in Figure 2a, and found in the flume experiments, the location of deepest scour, d_{Smax}, was a radial distance, R, out from the abutment column. For the present study (and many abutment embankments), the constructed embankment slope was 2 horizontal to 1 vertical, such that the requirement for embankment slope stability, when the slope extends back to the abutment column, is

$$\theta_S = \tan^{-1}\left(\frac{E_H + d_{S\max}}{R}\right) \tag{1}$$

where E_H is embankment height. Adjusting Eq (1), gives an estimate for the limiting values of d_{Smax};

$$d_{S\max} = R\tan\theta_S - E_H \tag{2}$$

The flume experiments showed that R varied with the abutment length parameter L/B_f (or essentially q_2/q_1), as indicated in Figure 3, which includes data from similar measurements reported by Barkdoll et al. (2007) who studied the use of riprap aprons as an abutment-scour counter-measure. The two data sets are in reasonably good agreement. Barkdoll et al. (2007) suggest for R,

$$\frac{R}{Y_f} = 4\left(\frac{L}{Y_f}\right)^{0.2} \tag{3}$$

Consequently, the limiting scour depth can be estimated as

$$d_{S\max} = 4\left(\frac{L}{Y_f}\right)^{0.2} Y_f \tan\theta_S - E_H \tag{4}$$

In other words, the maximum scour depth at the abutment should not exceed the limit given by Eq (4). Note that this limit can actually be attained, especially when θ_S is large, such as for an earthfill embankment formed of a compacted stiff clay. A larger scour depth leads to breaching of the embankment and flow relaxation through the bridge waterway (Figure 2b). The limiting scour-depth analysis should be further investigated for a range of earthfill materials, along with varying combinations of compacted embankment earthfill and floodplain soils. The present study was limited largely to uniform noncohesive sediment. The foregoing formulation of Eqs (1) through (4) is somewhat simplified, but is nonetheless indicative of how to estimate a limiting scour depth.

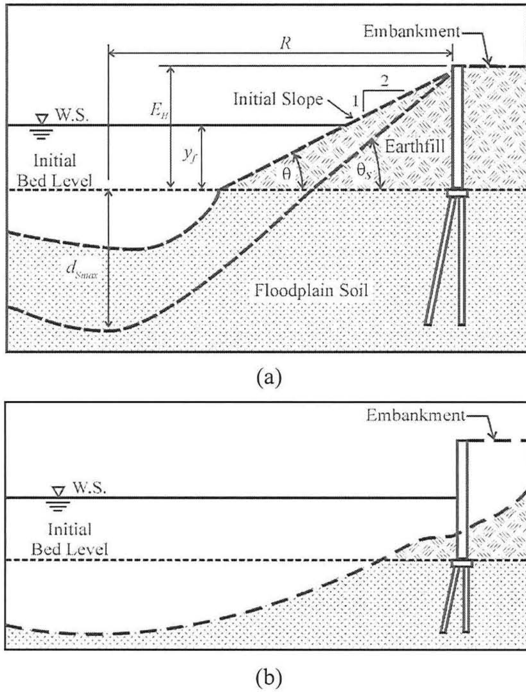

Figure 2. Deepening scour destabilizes the embankment face, causing the slope to fail geotechnically, and to erode back to a limiting condition. When the slope erodes back past the abutment column, the embankment breaches, and Scour Condition B attains an equilibrium state: the scour limit for an embankment face eroded back to an extent defined in terms of angle for embankment-slope stability, θ_S, and column position (a); and, embankment failure beyond this limit induces leads to embankment breaching and flow relaxation (b).

It could be noted for an analysis of abutment geotechnical stability that riprap presence does not enhance geotechnical stability. Riprap adds weight to the slope, but does not increase the shear strength of the earthfill forming the embankment.

For abutments on footing foundations, a limiting maximum scour-depth coincides with the undermining of the footing and the possible geotechnical collapse of the earthfill embankment behind the abutment column. This limit also could be formulated, at least in approximate terms. A formulation is not given here, but the photo shown subsequently in Figure 4 for a vertical abutment illustrates such a geotechnical collapse, and directly indicates how the formulation might be formulated.

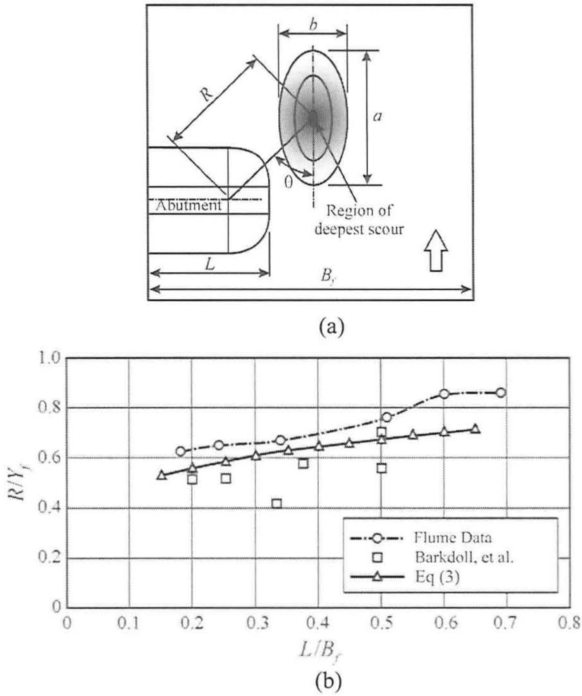

Figure 3. Definition sketch for distance, R, to deepest scour (a), and variation of R/Y_f versus L/B_f (b).

CONCLUSIONS

The new design approach replaces the old notion of treating abutment scour as a hydraulic erosion problem with the arguably more accurate notion that abutment scour essentially is a geotechnical problem. Most abutment failures are geotechnical failures, which limit the depth to which scour can develop. This paper offers a simple formulation for estimating scour-depth based on the geotechnical stability of the abutment spill-slope. Additionally, this paper presents photos of abutment scour illustrating the geotechnical failure of abutments. The limiting scour depth at bridge abutment for spill-through abutments is given by Eq (4).

Moreover, the study shows that limiting scour depth does not depend on arbitrary assumptions about combining bridge-waterway contraction scour and local scour at the abutment structure, a notion that the study's flume experiments do not support. Rather, the study shows that abutment scour is essentially scour at a short contraction, for which the combined influences of non-uniform distribution of flow passing around an abutment, and the generation of large-scale turbulence in flow, passing around an abutment are intrinsically linked.

Figure 4. This photo illustrates the importance of embankment strength with respect to the development of abutment scour: the slope failure of the embankment immediately behind a wing-wall abutment founded on a spread footing.

ACKNOWLEDGMENT

The investigation reported herein was conducted for National Cooperative Highway Research Program (NCHRP) under Project 24-20.

REFERENCES

Barkdoll, B., Ettema, R., and Melville, B. (2007). "Countermeasures to protect bridge abutments from scour." *Report 587, National Cooperative Highway Research Program,* NCHRP 24-18, Transportation Research Board, Washington, D.C.

Ettema, R., Nakato, T., Yorozuya, A., and Muste, M. (2008). "Three abutment scour conditions investigated with laboratory flumes," *Proc. of the 4th International Conference on Scour and Erosion (ICSE-4)*, Paper No. A-18, Tokyo, Japan, November 5-7, pp. 208-213.

Ettema, R., Nakato, T., and Muste, M. (2010). "Estimation of scour depth at bridge abutments," *Draft Final Report, National Cooperative Highway Research Program,* NCHRP 24-20, January.